INVESTIGATION ON CORTICAL BONE GRINDING USING ULTRASONIC ACTUATIONS

A Thesis Submitted in Fulfillment of the Requirement for the Award of the Degree of

MASTER OF ENGINEERING

in

Production Engineering

Submitted By

AMANPREET SINGH

801685001

Under Supervision of

Dr. Vivek Jain
Associate Professor
Mechanical Engineering Department

Dr. Dheeraj Gupta
Associate Professor
Mechanical Engineering Department

MECHANICAL ENGINEERING DEPARTMENT

THAPAR INSTITUTE OF ENGINEERING & TECHNOLOGY

(A DEEMED TO BE UNIVERSITY), PATIALA, PUNJAB

JUNE, 2018

Dedicated To My Grandfather

Late Sr. Bahadur Singh

CERTIFICATE

I hereby declare that the thesis entitled "**Investigation On Cortical Bone Grinding Using Ultrasonic Actuations**" is an authentic record of my work carried out as requirements for the award of the degree of **Master of Engineering** in **Production Engineering** at **Thapar Institute of Engineering and Technology, Patiala** under the supervision of **Dr. Vivek Jain**, Associate Professor, Mechanical Engineering Department, TIET, Patiala and **Dr. Dheeraj Gupta**, Associate Professor, Mechanical Engineering Department, TIET, Patiala during July, 2016 to July, 2018. No part of the matter embodied in this report has been submitted to any other university or institute for the award of any degree.

Amanpreet Singh

Amanpreet Singh

Date: 13/08/2018

Place: Patiala

This certifies that the above statement made by student is accurate according to the best of my knowledge and beliefs.

13/8/18

Dr. Vivek Jain
Associate Professor
Mechanical Engineering Department
TIET, Patiala-147004

13/08/2018

Dr. Dheeraj Gupta
Associate Professor
Mechanical Engineering Department
TIET, Patiala-147004

Acknowledgement

Though this dissertation work belongs to me, but there are many people who effortlessly worked with me to complete this work. I would like to thank all those people who made this thesis possible and an unforgettable experience for me.

First of all, I would like to express my deepest sense of gratitude to my supervisor Dr. Vivek Jain, who offered his continuous advice and encouragement throughout the course of this thesis. I thank him for the systematic guidance and great effort he put into training me in the scientific field.

I would like to express my very sincere gratitude to my second supervisor, Dr. Dheeraj Gupta, for his excellent guidance, caring attitude, patience, and providing me with an excellent atmosphere for doing research.

A special thanks to Dr. Vikrant Khullar, who allowed me to use Thermal IR camera. I am also thankful to Dr R.K. Duvedi for allowing me to work in CNC machine lab. I would also like to thank Mr. Ankit Sharma who helped me in my work whenever I needed.

I want to thank my friends, Amandeep Singh Tamber, Dilkaran Singh, Anirudh Singh Chana, and Daljeet Singh who created a friendly environment around me and kept me motivated and helped me in my research work also.

Finally and importantly, I take this opportunity to express the profound gratitude from my deep heart to my beloved parents and my brother for providing me with unfailing support and continuous encouragement throughout my years of study and through the process of researching and writing this thesis. This accomplishment would not have been possible without them. And at the last, thanks to almighty who helped me accomplish my research work through his presence in many forms, above mentioned persons are some of them.

Abstract

Bone burring has been in regular use in various surgical operations with its high demand. To minimize invasions of the surgeries and to increase preciseness of the grinding, there is continuous advancements in surgical methods in field of orthopaedic, dental and neuro surgeries. One such novel method that utilizes burring with assistance of ultrasonic vibration is known as abrasive coated rotary ultrasonic burring (ACRUB). Thermal and mechanical injuries to the bone tissue are the main concern in bone burring.

Abrasive coated rotary ultrasonic burring (ACRUB) is a non-traditional machining process that combines rotary ultrasonic process with computer numerical control (CNC) machine. It comprises of a piezoelectric transducer attached to a rotary spindle with diamond bur connected to give rotary and ultrasonic motion to bur. No study has been reported on ACRUB of bovine bone.

The aim of this thesis was to provide a surgical method to grind the bone with ACRUB and reduce the thermal damages and normal force to aid in removing thermal necrosis of the tissues. A Taguchi L9 method was applied in dry conventional grinding (DCG) of bone with input parameters as spindle speed, feed-rate and depth of cut. An optimum set of parameters was obtained and then in next study, these parameters were considered to compare dry ACRUB with DCG in which half ACRUB and half DCG was done in 5 mm length of cut. Then same parameters were tested with ACRUB with coolant. It was observed that ACRUB is superior to DCG, and temperature about 25 °C was obtained which remove any chances of thermal necrosis.

Keywords: Bone burring, Cortical bone, Abrasive coated rotary ultrasonic burring, Taguchi L9 experiment, Thermal Necrosis

Table of Contents

List of Figures

List of Tables

List of Acronyms

Acronym	Full name
CNC	Computer numerical control
RUM	Rotary Ultrasonic Machining
CM	Conventional Machining
NCM	Non-conventional machining
USM	Ultrasonic Machining
MRR	Material Removal Rate
FEM	Finite Elements Methods
CFRP	Carbon Fiber Reinforced Plastics
FETM	Finite Element Thermal Models
EGW	Elemental Grinding Wheels
ACRUB	Abrasive Coated Rotary Ultrasonic Burring
DCG	Dry Conventional Grinding
SEM	Scanning Electron Microscope
IHTM	Inverse Heat Transfer Method
FEPA	Federation of European Producers of Abrasives
ANOVA	Analysis of Variance

List of Symbols

Symbol	Meaning
°C	Degree Celsius
s	Spindle speed
f	Feed-rate
d	Depth of cut
N	Newton
mm	Millimeter
µm	Microns
mL/H	Millilitres per hour
Hz	Hertz
mm/min	Millimeter per min
rpm	Revolutions per min
fps	Frame per sec
W/mK	Watts per meter-Kelvin
MPa	Mega Pascal
GPa	Giga Pascal
k	Thermal conductivity
c	Specific heat
T	Temperature
F_Z	Normal force
T_{avg}	Average temperature
F_{ZAvg}	Average normal force
db	decibels
Si_3N_4	Silicon Nitride
ε	Emmisivity

Chapter 1

Introduction

1 Introduction

1.1 Project Background

The grinding of teeth in dental practice, bone in the neuro-surgical brain surgery and plaque inside blocked coronary and peripheral artery are some evidences that abrasive processes are prevalent in medicine sector. Bone burring has become a crucial surgical procedure for neurosurgery and orthopedic surgery. Taking the example of minimally invasive surgical procedure called endoscopic endonasal burring to easily approach the skull base, in which the nostril is used as a pathway to reach the internal area of skull without spoiling the surgical cut made. Neurosurgeons happens to be using the mini ball-shaped diamond grinding wheel , 3-4 mm in diameter, to cutout the bone and gain the access for surgical operating of the tumor. But they also need to operate with utmost care, protecting the cranial nerves. High rotational speed wheels are used in such surgical endoscopic operations.

During bone burring, there is generation of heat which conducts via bone to the surrounding nerves network and blood vessels. It is a well-known phenomenon in medical region that upsurge in temperature of the bone, nerve, and artery can cause thermal-related injury such as blood coagulation, which can lead to strokes, and bone necrosis. Necrosis occurs because the osteoblast cells dies due to heat and thus there is no replenishment of bone cells which are destroyed by osteoclasts. A study reports that when the temperature of the bone is raised above 43°C during continuous grinding by diamond wheel, thermal necrosis occurs due to irreversible death of the bone cells, even with extensive saline irrigation (720 mL/H). This has adverse effects on bone regeneration and healing [1].

To prevent thermal injury, minimization of temperature rise is the necessity. Most neurosurgeons prefer diamond bur instead of steel cutting burs because they offer very less trauma with higher resistive force but this resistive force converts to heat. Machining by plastic deformation, though

preferred for better accuracy, usually leads to increase in cutting temperature which increases the risk of thermal damage to the bone [2]. Currently, the saline irrigation is the primary cooling method. Also displayed in this study on bone flaps grinding, under no cooling system, the maximum grinding temperature of a diamond wheel is about 1.5 times that of stainless steel tool, and about 1.2 times under saline flooded irrigation [1]. This is due to the conspiracy of high speed surgical wheel and congested surgical space in the skull bone burring which limits the effect of saline cooling and, thus, there is a need for advancement in surgical burring devices.

For reduction in temperature and for precise motion and control of tool, there is requirement of a new burring system which is robot controlled and will assist in minimizing the burring temperature of bone. If the time period of exposure to high temperature is small then even if the temperature is greater than the critical temperature, chances of thermal necrosis are reduced [3–8]. Therefore, an attempt has been made to mimic the robotic system using computer numerical control (CNC) vertical milling machine with ultrasonic assisted abrasive tool (RUM) and proper irrigation system and also the effects of various machining parameters were also studied.

Thus, the proposed innovation is concerned about the specific problems of burring of human cortical bone and develop a burring system which produces very less axial force, eradicate thermal necrosis and also very less cracks formation.

1.2 Classification of bone machining techniques

Bone machining techniques can be classified into two categories: conventional (CM) and non-conventional machining (NCM), as shown in Figure 1.1.

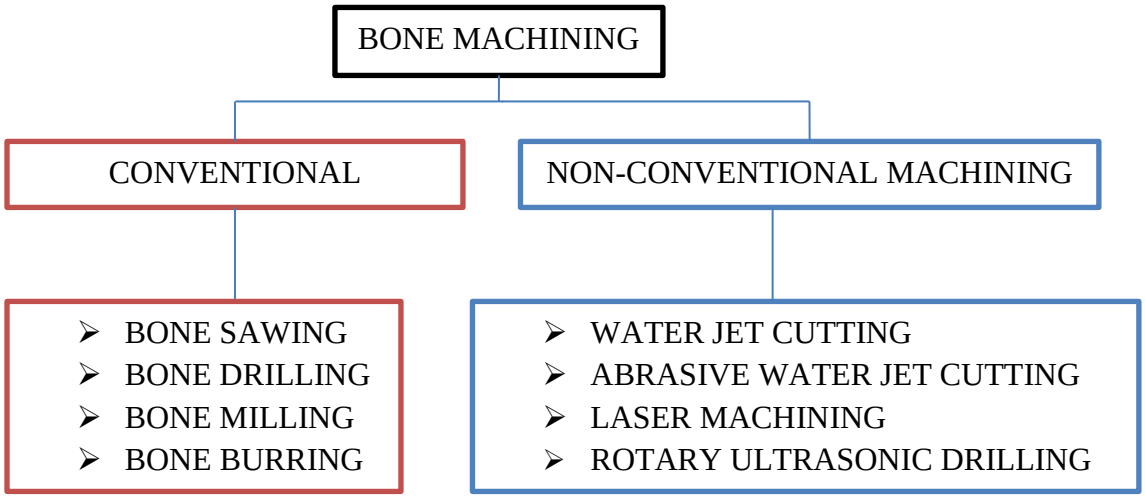

Figure 1.1: Current techniques for bone machining [9]

Conventional machining- In this removal of material takes place mostly in the form of chips with the help of a wedge shaped cutting tool applying forces on workpiece resulting in plastic deformation internally and leading to deformation with shear force along the shear plane and forming of chips. The tool used is harder than workpiece. Bone sawing, Bone drilling, Bone milling and Bone burring are part of CM.

Non-conventional machining- These are the modern era techniques used for machining in which there may be chip formation or no chip formation during material removal. This can be seen in abrasive water jet machining where micro sized chips forms but in electrochemical machining, electrochemical dissolution at atomic level results in material removal. There are possibilities of absence of tool physically, which can be evident from laser machining where laser beam is used. It is not necessary that tool should be harder than material of workpiece.

The basic differences between these two types of machining can be made on the basis of tool wear, precision and accuracy, environmental effects, tool life, cost, skill requirement, complexity of setup and availability of spare parts, as shown in Table 1.2.

Table 1.1 Difference between CM and NCM.

S.NO	FACTORS	CM	NCM
1	Tool wear	High wear rate	Very low wear rate or no wear in many cases
2	Precision and Accuracy	Less than its counterpart	More accurate and precise
3	Environmental effects	Results in noise pollution.	No noise pollution.
4	Tool life	Short tool life due to physical contact between tool and workpiece.	Long tool life due to absence of any contact.
5	Skill requirement	No skill requirement.	Training is necessary.
6	Setup	Simple	Complex
7	Availability of spare parts	Easily available.	Not easily available.
8	Cost	Cheaper than NCM.	Very expensive.

1.3 Rotary ultrasonic machining (RUM)

The mechanism of material removal of conventional diamond grinding and static ultrasonic machining (USM) combines to form non-conventional hybrid machining process, named as RUM, which leads to a material removal rate (MRR) higher than that would have been attained individually by them. RUM leads to the removal of material from workpiece with the help of micro-chip machining and grind action of grits [9].

A diamond abrasive tool is assisted with ultrasonic vibration of 20,000 Hz and feed is given continuously towards the workpiece. The pumping of coolant is done continuously through a nozzle towards the tool-workpiece interface, which flushed out the debris, preventing rise in heat, and keeps the cutting zone cool.

The characterization of work piece for RUM is usually done by properties of high hardness and brittleness. This implies that other material properties such as electrical conductivity and chemical reactivity has no effect on machinability of a material. RUM is a non-thermal, non-chemical and non-electrical process. Due to this, there is no change in physical, chemical or metallurgical properties of the work piece post machining [9]. It has been reported that in

vibration assisted machining, the use of ultrasonic vibrations reduces the stresses and the subsurface damage developed in the workpiece. As a result the strength of the workpiece after machining is maintained. The cutting forces developed are lower during vibration assisted machining compared to conventional grinding [10]. In ultrasonic machining, the heat generated in the machining zone is not very high [11].

1.3.1 Principle of Working

The machining setup consists of ultrasonic assisted spindle system, a data acquisition system, and an irrigation system [9]. The ultrasonic system is a combination of an ultrasonic spindle, with a transducer, electrical motor with a power supply unit. Sine-wave generator with high power capacity, converts low frequency (50 - 60 Hz) electrical signal into high frequency (20,000 Hz) electrical signals which is further received and converted into linear mechanical vibrations of high frequency by piezoelectric transducer. Generally, the conversion efficiency up to 96 % is attainable in piezoelectric transducer which is the reason it has been preferred and requires lesser cooling which competes with magnetostrictive type transducer having 20-30% efficiency. Piezoelectric transducer has low noise levels, thus, improving workability.

The power supply output is responsible for adjusting vibration amplitude. An electric motor attached to the ultrasonic spindle controls the rotational motion of cutting tool, having capability to run at different speeds by adjusting its rpm. A data acquisition system such as dynamometer can be used to measure cutting forces and torque during machining. This also consists of a computer system which records and plots the measured data. The coolant system involves pump, fluid tank, pressure gauges, control valves, and pressure regulator. Its purpose is to supply coolant fluid at the machining zone and keep it cool.

1.3.2 Mechanism of Material Removal

The mechanism involves three actions by the tool; hammering, extraction, and abrasion, as shown in Figure 1.2 [9].

1. The hammering action is the result of indentation of abrasive with crushing act on work material beneath the impact of ultrasonic vibration.
2. The abrasion action is caused due to rotational motion of diamond tool.

3. The extracting of material is due to combined action of rotational and vibrational motion of tool.

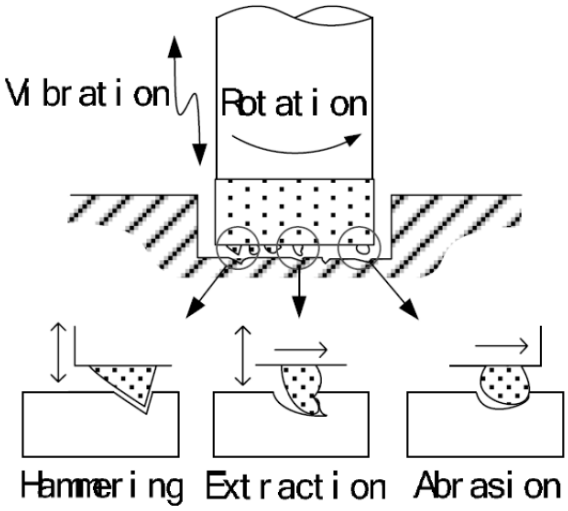

Figure 1.2: Mechanism for RUM [9]

A study was conducted on surface topography to draw out the mechanisms responsible for material removal [9]. A leading mode of material removal was found to be brittle fracture of work surface. This was due to the above three actions of tool. Out of these, hammering action was dominant in removing of material, whereas walls of machined area were ruled by abrasion action. These both actions lead to swarf formation, which mixed up with the pressurized coolant fluid resulting in extraction action at walls of machined area.

1.3.3 Advantages of RUM

- RUM helped to remove some drawbacks of the ultrasonic machining process: low MRR and inaccuracies in machined holes like out of size holes and oval defect [9].
- It becomes difficult to achieve close tolerances due to presence of abrasive slurry causing erosion of surfaces in machined hole walls, potential reason being debris escaping out and suspended abrasive grains during their flushing [9].
- The abrasive tool enhanced hole accuracies with ease to drill larger length to diameter holes.
- The impregnation of abrasive slurry on tool tip resulted in exploring RUM process for applications in various fields of industries.

RUM is one of the economical and environment-friendly machining processes which could be applied for the machining of advanced hard materials with improved machining accuracy, extremely tight tolerances, very low surface roughness, and higher MRR.

1.3.4 Applications

Rotary ultrasonic machining has a wide range of applications in areas such as aircrafts, automobiles, sports goods, medical tools, computers, electronics, optical, etc.

- In automotive and optical industries, Zirconia and glass ceramics are discernible advanced materials suitable for machining with RUM.
- Carbon fiber reinforced polymer (CFRP) composites machined through RUM is popular in aircrafts, automotive industries and fabrication of engine blades is also accomplished using them.
- RUM has attained feasibility in machining of titanium and its alloys, applicable broadly in the parts formation of turbines such as; rotors, stator and compressor blades etc.
- A wide variety of engineering materials are easy to machine by RUM process, since it's not affected by limitation of any properties of work material to be machined. The success has been achieved in RUM machining of Stainless steel.
- Sapphire, easily found in the fabricating of electronic circuits, has been processed through RUM.
- The ability of RUM of precision processing of brittle materials is utilized in machining of K9 and BK7 glass.
- The RUM can be collaborated with other processes like grinding which further enhanced its application area [9].

1.4 Bone

Bones at first glance looks lifeless but are active and living tissues being remodeled constantly. It is a composite tissue having hard outer layer made of crystalline calcium phosphate (hydroxyapatite) with small amounts of other mineral substances, covering a soft spongy structure made of the protein collagen. Outer layer gives strength and inner honeycomb-like structure containing matrix gives flexibility required by the body. With structurally supporting the body, it also protects vital organs. They also help with providing an environment for bone marrow to create blood cells. They also act as storage banks of many minerals such as calcium.

The bones are stiffer and stronger at higher strain rates, which is a way to compensate for the higher loads and stresses imposed by vigorous activity or super physiological loading.

1.4.1 Structure of bone

Macroscopically, bones consist of two types of tissues: cortical and cancellous bone. Porosity is the primary feature to distinguish between these two bone types, with cancellous bone higher in porosity. Cortical bone is considered to have relative density greater than 0.7, which reflects the presence of minor amounts of porosity, while it is lower than 0.7 in case of cancellous bone.

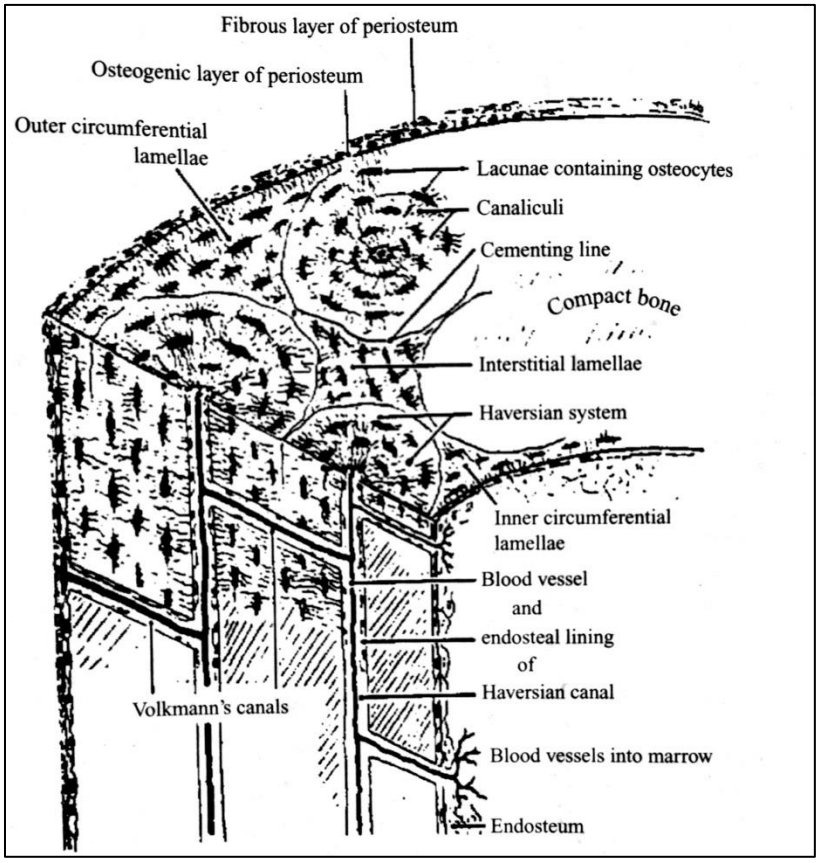

Figure 1.3: Microstructure of cortical bone. [12]

1. Cortical bone (Compact bone) - It is the outer hard layer which is strong, dense and durable. It is about 4/5th of adult bone mass. Its function is to give supportive strength to the body, give protection to organs, to reserve and liberate chemicals such as calcium. At micro-level, its structure is complex which plays a crucial role in its mechanical properties. It is laid down in 5 µm thick layers called lamellae. The collagen fibers run parallel to one another within these layers but with different orientation compared to other layers. The arrangement of lamellae is in

different ways in various parts of bone (Figure 1.3). Close to the outer and inner surfaces of bone, there is circumferential arrangement of lamellae parallel to one another, known as circumferential lamellae. In between, there exist cylindrical-shaped structures, approximately 10 mm long and 0.2 mm in diameter, formed from concentric lamellae, named as osteonal bone, which is aligned with the long axis of bone. A highly unified network of canals and channels is suffused in this solid bone matrix. These networks contain osteocytes, where extracellular fluid supplies dissolved nutrients to them. Concentric lamellae surround *Haversian canal*, through which a blood vessel runs. Then there exists microscopic channels called *canaliculi*, which helps to connect central canal to these lamellae. The group comprising a canal, surrounding lamellae and intervening bone is termed as an osteon (Figure 1.4). The packed osteons become a proper bone having in between space called *interstitial lamellar bone*. There is the junction between interstitial bone and osteons named as *cement line,* which is less than 1 µm in thickness. It is a layer which is highly mineralized and collagen-free. Due to above features cortical bone gets strongly anisotropic properties i.e. greater stiffness and strength will be developed along the axis of cortical bone rather than properties in perpendicular direction to the bone's axis. Also it is stronger in compression than in tension [12].

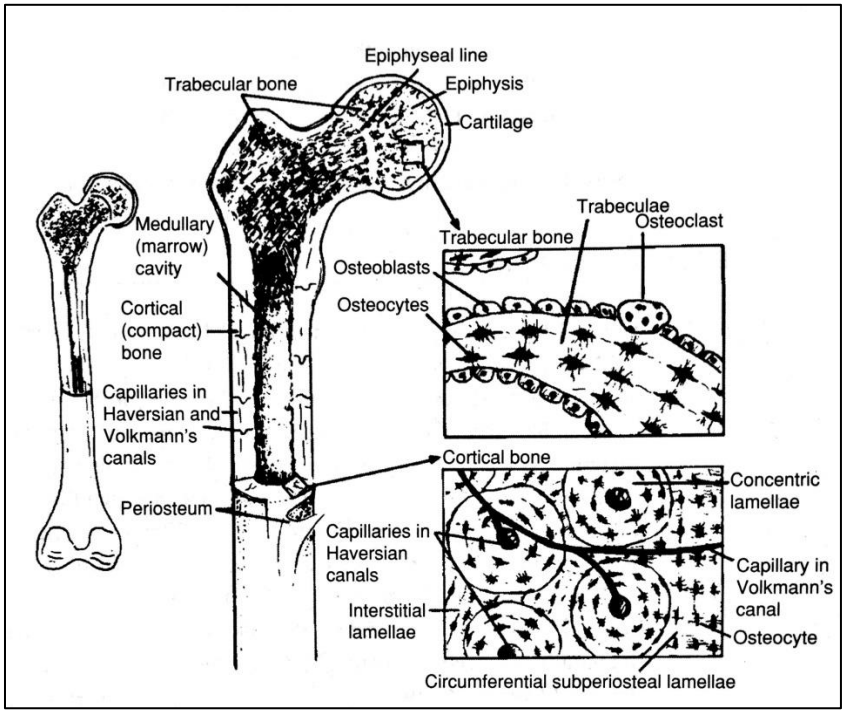

Figure 1.4: Overview of bone architecture with cortical and trabecular bone positions [12]

2. Cancellous bone (Trabecular bone) - It is a network of rod-like structures which is lighter, and more flexible than compact bone. The vertebrae as well as the ends of the long bones do contain them such as the femur, tibia, and radius. It has a lamellar structure same as cortical bone, with lamellae running parallel to the trabeculae. The difference is the matrix organization with struts interlinked as a three-dimensional porous network called trabeculae which is filled with bone marrow. In healthy bone, trabeculae are on average about 0.2 mm thick [12].

1.4.2 Types of bones

Bones are classified on the basis of shape. These are:

1. Long bones: There length to width ratio is very high. The primary way of growth is the diaphysis gets elongated, with epiphysis at each end of the growing bone. These bones facilitates in supporting weight and help in body movements. Femur and tibia are examples of long bone.

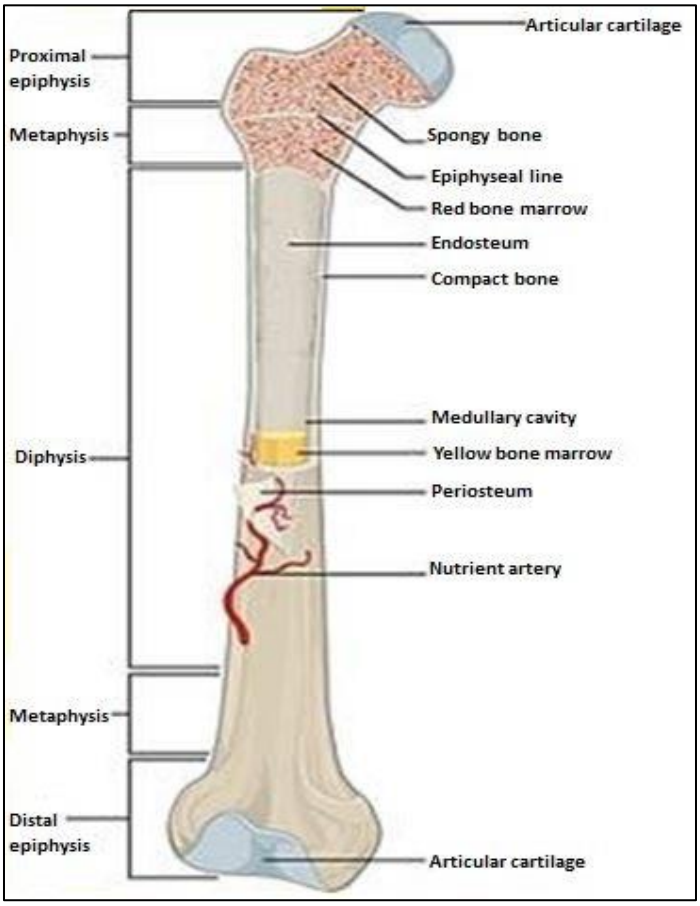

Figure 1.5: Structure of long bone (Femur). [13]

2. Short bones: These are nearly box-shaped with a thin layer of compact bone surrounding a spongy internal structure. There is absence of medullar cavity with length to width ratio very low. Their examples are wrist and ankle bones.

Figure 1.6: Short Bone (Carpal). [13]

3. Flat bones: These are curved and thinner in shape. A layer of spongy bone is sandwiched in between two parallel layers of compact bones. Breastbone and most of the skull parts are flat bones.

Figure 1.7: Flat Bone (Skull). [13]

4. Sesamoid bones: Tendons constitutes these bones, such as patella or kneecap. Their role is to protect tendons from stress and wear.

Figure 1.8: Sesamoid bone (Patella). [13]

5. Irregular bones: These are bones with unusual shape and do not fit into the previous four categories discussed. These are the bones of spine and pelvis. Their function is to protect organs or tissues.

Figure 1.9: Irregular bone (Vertebra). [13]

1.4.3 Bone cells

Various types of bone cells are shown in Figure 1.10:

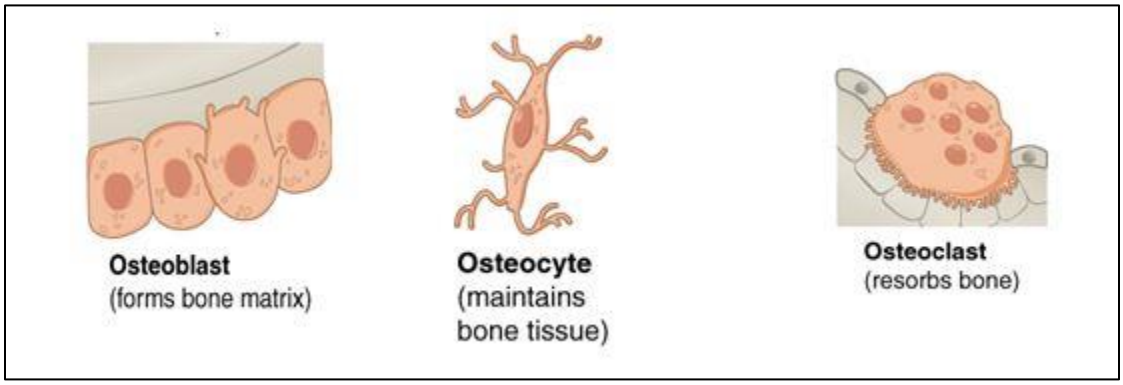

Figure 1.10: Bone cells. [13]

1. Osteoblasts- These are the 'builder' of bones. These are mono-nucleate bone forming cells. They are found closer to the bone surface and helps in production of protein mixture known as osteoid, which accumulates and gets harden to result in bone formation.

2. Osteoclasts- These are 'destructor' of bones. These are very large multinucleate cells responsible for resorption of bones. These are cells with multiple nuclei located on bone surfaces in resorption pits called as *Howships lacunae*. They demineralize the adjacent bone with acids by dissolving its collagen.

3. Osteocytes and lining cells- These are created from osteoblasts embedded in the bone matrix during their process of secretion, making them inactive, while lining cells are found residing on bone tissue upper layer. Both are connected by small canals, helping them in communication.

Osteocytes get trapped and surrounded by bone matrix produced by them. Lining cells resides on the bone surface when formation of bone stops.

Osteoblasts and Osteoclasts are the crucial parts of bone remodeling cycle. One makes and other creates, that means continuous change in bone structure takes place with repair of bone cells.

1.4.4 Bone properties

Bone is hierarchical, has a varying macrostructure with anisotropic properties. Due to this it develops high compressing strength, poor tensile strength with very low bearable shear strength (Table 1.1). The elasticity is mainly contributed by collagen as cortical bone is brittle.

Table 1.2 Mechanical properties of human cortical bone. [12]

Parameter	**Value**
Modulus (in GPa)	
Longitudinal	17
Transverse	11.5
Shear	3.3
Poisson's ratio	0.3-0.6
Ultimate strength: longitudinal (in MPa)	
Tension	133
Compression	193
Shear	68
Ultimate strength: transverse (in MPa)	
Tension	51
Compression	133

In thermal properties, the most important characteristics are specific heat (c) and thermal conductivity (k). Specific heat is the amount of heat per unit mass required to raise the temperature by one degree Celsius. Thermal conductivity is the ability of the material to conduct heat. From many researches it has been found that cortical bone is thermally anisotropic and has high conductivity and diffusivity in axial direction than in the lateral direction. For human bones thermal conductivity was found to be varying from 0.3-0.38 W/mK. For bovine bones, it is about

0.58 W/mK in longitudinal direction, 0.54 W/mK in radial direction and 0.53 W/mK in circumferential direction [12].

1.5 Summary of the chapter

This chapter begins with background of project. The classification of bone machining techniques based on conventional and non-conventional machining was also discussed. Furthermore, the mechanism of RUM, advantages, and applications is explained. This chapter also discussed briefly about bone, bone types and its properties.

Chapter 2

Literature Review

2 Literature Review

2.1 Review of the existing literature

2.1.1 Drilling

Matthews and Hirsch [8] investigated the elevated temperatures while drilling in cortical structure of human femur at several rates of rotation and at several level of drill pressure with elevated temperature durations at specific distances with respect to the drill hole wall. They also studied the effects of using forced and manual irrigation, of predrilling, of a drill guide, and also of tapping. They recorded greater cortical temperatures, succeeding 100 degrees centigrade, when drilling without a proper coolant system. In case of both the magnitude and duration of elevated cortical temperatures, the applied drill force was found to be more dominant factor than drilling speed. It was observed that when drill force was increased, it lead to decrease in maximum temperature and duration of temperature elevations. A greater change in temperature caused due to worn drills as compared to new drills. It was found that any form of irrigation is effective only when fluid stream is allowed to be directed at the penetration point of cortex. Also, no significant increase in temperature appeared while tapping.

Li *et al.* [14] investigated the conduction of heat in bone drilling by establishing a finite element method (FEM) based three-dimensional model focusing on feed rate, spindle speed and drill diameter. They revealed that if any of three parameters rises, it will increase the drilling temperature. Then an empirical formula was given by them to predict the temperature and to optimize the parameters. They also introduced the idea of intermittent feed drilling, to be more effective in reducing thermal necrosis to bone tissue.

Fernandes *et al.* [15] studied the real-time temperature changes, with different parameters, during the drilling of bovine bones and polyurethane foam blocks. They tried to make a comparison between the results produced by drilling different materials with similar machining

conditions, to get assurance level with a similar trend of conclusions. They tried to demonstrate that temperature can be reduced far below the critical values if an optimized set of drill parameters are implemented. They concluded that lower will be the increase in bone temperature, if higher are the drill speed and the feed-rate and with increase in depth of hole leads to maximum drilling temperature. They presented that temperature value was lower in case of bone tissue than in the solid rigid polyurethane foams. Based on this study, they suggested high drill speeds, high feed-rates and the reduction in contact area between the bone and drill.

2.1.2 Grinding

Shih *et al.* [16] presented an inverse heat transfer method (IHTM) to speculate the temperature at bone grinded area in neurosurgery. With this method (i.e. IHTM) the thermal power of grinded area was quantified. Then this approach was used to perform a FEM thermal analysis on a 3-D skull model based on a patient-specific CT and MRI images of skull using software package ABAQUS Standard V6.8, in which thermal power of 0.52 W was applied to the surrounding bone when operating near optic nerve. The results showed that grinding temperature exceeds the threshold temperature (50°C) at the optic nerve and that indicates thermal injury.

Kei-lin *et al.* [17] performed experimental investigations on glass with the application of RUM milling and presented a tool design method. They found increase in surface roughness at the entrance and exit region with increase in feed rate and depth of cut. Also, the milling resistance increased, which accelerated the tool wear. But at a certain level, it results in slight decrease of surface roughness, which is due to decrease in cutting angle and grit size. However, the surface roughness increases caused by excessive resistance and tear out of grits due to which direct contact is established between work material and coated tool surface. Also, greater process rate was observed due to reduction in milling resistance by ultrasonic tool vibrations. But, the micro crushing act due to assistance by axial ultrasonic vibrations on work material, damages the milled surface. The tool design method increased the surface roughness on one hand but the change in tool angle enabled the ultrasonic milling on other hand by increasing the ultrasonic kinetic energy.

Zhang *et al.* [18] developed a method to make temperature distribution the logical quantity during the bone grinding. This method included an IHTM for heat determination and a three-dimensional FETM thermal model for spherical grinding tool. In 3D FETM model, the spherical

grinding tool is disintegrated into EGWs and each one has the ability to grind individually such that a 3D heat flux distribution is created. To calculate the unknown rate of heat generated, an optimized algorithm was utilized by the IHTM to match the developed FETM model with the experiments, also, which validating its accuracy. The temperature rise during grinding could be easily understood by this study and they gave demonstration of the high thermal injury potential in about 3mm region from the point of tool-bone interaction during grinding in absence of cooling system.

Tai *et al.* [19] developed a method which used electrical power of motor as an input to monitor the temperature in procedure of neurosurgical bone grinding. They utilized a heat conversion model with a finite element analysis (FEA) based thermal model to estimate temperature. The heat generated was determined using the linear correlation of the heat conversion model to the motor power. Then superficial temperature of bone is calculated by the FEA thermal model using the heat obtained by previous method.

Zhang *et al.* [20] proposed a cryogenic saline mist system which dominated the conventional flood irrigation system in minimizing the thermal necrosis with enhancing the vision of surgeons. They suppressed the bone temperature rise by delivering a cryogenic mist directly towards the grinding area along with backward grinding motion, which helps to achieve local maximum cooling effect. But in forward grinding motion, the coolant system was above the tool due to that the concentration of coolant was not at the bone-tool interface, which increased the temperature very high above the injury threshold temperature. A pre-cooling effect was observed that aids in reduction of bone initial temperature prior operation.

Enomoto *et al.* [21] found that coating diamond wheels with submicron-sized titanium dioxide particles enhances the hydrophilic nature of the wheel surface due to which the surface adsorbed only water molecules and helped maintain the cooling effect and protecting tool from bone swarf thus suppressing the bone temperature rise during the grinding as compared to commercially available tool.

Egashira *et al.* [22] attempted to drill holes of diameter less than 100 microns by grinding in crown glass. They fabricated micro pins of cemented tungsten carbide by electrical discharge machining, in which small convex-shaped craters act as cutting edge of abrasive grains found in

grinding wheel, to use them as micro-grinding tools. They employed ultrasonic vibrations to the workpiece, to prevent tool breakage by reducing the grinding force. With the aforesaid implementation, the microholes down to 0.01 mm in diameter were easily drilled by them. They drilled three holes of 30 µm, 20 µm and 10 µm, respectively. They found that in first case, holes were taper with no reduction in grind force on using helical feeding, in second case, holes were again taper in shape with reduction effect of grinding force with helical feeding but it couldn't prevent tool breakage, which revealed unnecessity of helical feeding. In third case, low aspect ratio tool was used without helical feeding, due to which tool breakage resistance improved, thus, enabling use of small diameter tools. They claimed to achieve the smallest-diameter hole, of 10 µm diameter, drilled by grinding.

Jianhua *et al.* [23] studied the influences on grinding forces and surface characteristics of ultrasonic assistance by theoretical and experimental methods on silica glass. They found that on intermittent cutting resulted in oscillating of instantaneous abrasive cutting thickness as analogous sine wave, which resulted in reduction of average value of instantaneous abrasive cutting thickness. They achieved significant reduction in grinding forces with normal grinding force up to 65.6%, tangential force about 48%, and 42.2% of cross feed directional grinding force. Larger depth of cut and feed rate due to positive effect of tangential grinding force with increase in grinding parameters improved machining efficiency and material removal rate. They found easiness in ductile machining, in ultrasonic assisted micro end grinding, as compared to conventional micro end grinding.

Shen *et al.* [24] conducted a study on diamond wheel wear characteristics by grinding the ceramic named alumina with and without ultrasonic vibration. The variations in surface topography of the wheel were captured with the force measurements. They found significant improvement in the self-sharpening property of diamond wheel by ultrasonic vibrations but caused great wheel wear. They showed that during grinding process ultrasonic vibrations also created micro cutting edges on the diamond grits, which keep on sharping the working area of diamond wheel without increasing the force ratio and grinding force.

Dillon *et al.* [25] presented a robot assisted milling of bone that used estimations of bone density based on images, locating vital anatomy by generating an efficient and safe plan of cutting. They controlled the cutting forces by regulating the incidence angle of the burr. Their aim was to

reduce the accidental collisions by preventing robot deflection towards the vital anatomy due to large forces with faster low density bone area milling. The method considers the local bone density with position of vital anatomic structures with respect to spherical burr, while selecting the tool orientation and cutting velocity. They made a comparative study between the robot milling and CNC-like bone milling, in which there was more reduction of mean and peak forces in the earlier one as compared to other, while reducing the machining time.

Wang *et al.* [26] mathematically estimated the areal effect of heat flux using experimental data in collaborating with inverse heat transfer method. The heat flux with temporal change is reflected in this inverse method by considering a time-varying system. To calculate the temporal and spatial variables, sequential function specification method (SFSM) was combined with sequential quadratic programming (SQP). To determine the ability and limits, numerical tests were performed for this method. To reconstruct the heat flux, a pre-work data was applied. Analyzing the results have proved that i) towards traversal direction of burr, a nearly triangular distribution was observed, ii) the magnitude of heat flux towards the direction of feed is higher, and iii) a null heat sink effect indicated by close enough time-invariant heat flux. The experimental setup dependent future time step (r) and the initial values of geometrical variables (k) influenced the inverse results.

Liu *et al.* [27] conducted orthogonal experiments on silicon nitride grinding with a diamond abrasive wheel to study the effects of the grinding parameters such as wheel speed, grinding depth, grain size, work piece speed on the grinding pressure, surface roughness, surface morphology, and subsurface damage. They found grinding force about 15 N/mm and the grinding force ratio lying in range 5-12 consonance with grinding characteristic of brittle material. Due to increase in the grain size number, tangential force meaningfully upsurges, which is bonus for material removal during grinding. They reflected a trend of brittle to plastic material removal by increasing the grain size, thus, reducing the pit area and its quantity. Similar results were observed with surface roughness and subsurface damage depth of grounded Si_3N_4. They increased with increase in depth of grinding and work piece speed but decreased with the rising grain size and wheel speed. Thus, they tried to improve the grounding efficiency and quality of Si_3N_4 by some optimization of the grinding parameters.

Yang *et al.* [28] studied microscale skull bone grinding temperature field under different irrigation systems. They created Micro-grinding model, heat flux density model, convective heat transfer coefficient model and intra-workpiece heat conduction model, collaborating them to simulate the microscale bone grinding temperature region under nanoparticle jet mist cooling system (NJMCS), mist cooling system, drip cooling system, and dry grinding system. According to simulation results, low temperature peak up to 27.5 °C was seen in case of NJMC, followed by mist cooling, drip cooling, and dry grinding successively. An experiment was conducted on fresh bovine femur bone using these different cooling conditions to verify the simulated results. It was observed that the temperature peak of NJMC is 26.2°C, which is 89.16%, 70.05%, and 62.98% of mist cooling, drip cooling, and dry grinding, respectively, verifying the optimal cooling effect of NJMC.

Paknejad *et al.* [29] conducted a thermal analysis on work material X20Cr13 with the application of longitudinal and transverse directed, ultrasonic vibration assisted dry creep feed up grinding. They saw a significant reduction in temperature when using ultrasonic vibration in comparison to conventional dry creep feed up grinding. They observed that there is increase in grinding temperature with increase in depth of cut in both conventional grinding and ultrasonic assisted grinding. Also, they found temperature reduction from 1.39% to 25.91%, when grind depth is varied from 0.2 to 0.6 mm. 16.51% temperature reduction was obtained under ultrasonic vibration at lowest feed rate of 100 mm/min. The ultrasonic effect becomes significant from 5.81% to 15.01% temperature reduction upsurge, when cutting speed decreases from 25 m/s to 15 m/s with the application of ultrasonic vibration at 0.3 mm grinding depth and 1000 mm/min cutting velocity.

Kusins *et al.* [30] presented a desirable outcome through the experimental quantification of the bone burring parameters, considering both optimized procedure and future implementation into the design of closed-loop controllers used in robot-assisted bone machining process. Also, they investigated the effects of different tools, tool rotational speed, feed-rate, depth of cut, cut overlaps, and tool angle on vibration, temperature, and cutting forces in cortical bone machining. They found that spherical tool is dominant over cylindrical tool, in that, the cylindrical tools should not be used unless the cutter approaches workpiece with positive or negative inclination angle. They performed bone burring using a 6 mm spherical burr suggesting the optimum

conditions i.e. rotational speeds reaching 15,000 revolutions per minute with feed-rates low as 2 mm/s and overlaps larger as 50% which yielded local minimum temperatures less than 30°C and vibration less than 3 g rms. They claimed this to be the best to avoid high temperatures/vibrations, providing the required feasibility of variably engaging with the bone without nulling the benefits of low thermal temperature and vibration outputs.

2.2 Summary of literature

- Several authors have studied the effect of drilling and grinding parameters on the surrounding nerves, tissues and bones. It was observed that temperature higher than the threshold temperature was recorded which leads to thermal necrosis. They tried to control the temperature rise with variation in parameters and optimizing them [15, 16, 18, 19, 20, 21, and 24].
- A few authors have studied the effect of various coolant systems on the grinding temperature. It was observed that nanoparticle mist cooling was dominating flood irrigation, drip cooling and mist cooling in reducing the temperature to lowest possible point. While, some developed burr with ability to increase cooling effect [20, 21, and 30].
- Most of the authors have made mathematical models and used them in simulation models and performed thermal analysis. They created the possibility of estimating the temperature generated which is practically not feasible [18, 19, 26 and 30]**.**
- Some authors have studied the effect of rotary ultrasonic machining on materials such as glass, ceramics, X20Cr13, excetra and compared it with the conventional machining. They found significant decrease in temperature and tool force during vibrational machining. They also studied the vibrational effect on tool wear [17, 22, 23, 25 and 29].

2.3 Gaps in the reviewed literature

- Although, authors have studied the influence of grinding parameters on grind temperature during conventional grinding but none have studied using the rotary ultrasonic grinding method.
- Many studies focuses on bone drilling but few studies made an attempt on bone grinding.
- Many authors developed simulation models to estimate temperature but did not considered the effects of coolant system used during surgical operations.

- Most of the authors performed experiments using only spherical abrasive burrs, but did not worked on improvement of the carbide cutting.

2.4 Problem Formulation

Ultrasonic actuations can be a high potential effect in grinding of the bone, instead of grinding with conventional means in neuro surgeries. Therefore, an attempt has been made in the present work to investigate the thermal effect and normal force effect of ultrasonic grinding on a goat bone.

2.5 Objectives

(i) To analyze the effect of input parameters on burring temperature during the experimental process.

(ii) To evaluate the normal cutting forces during the DCG and ACRUB process.

(iii) To make a comparison between ACRUB and conventional grinding of bone.

(iv) To perform SEM analysis and thermal analysis on burred portion of cortical bone.

2.6 Methodology

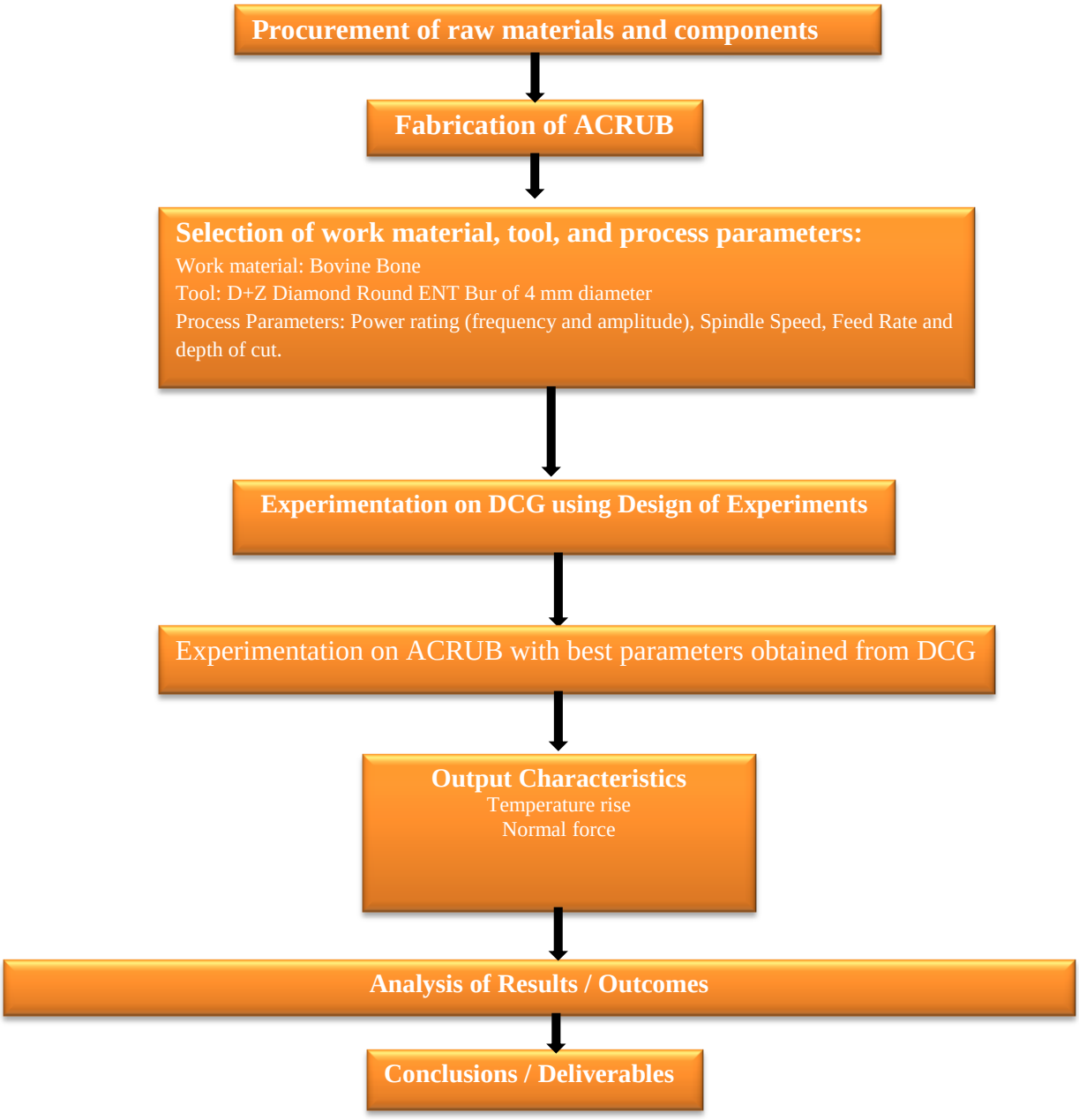

Figure 2.1: Methodology used for research work.

Chapter 3

Experimentation

3 Experimentation

3.1 Experimental Details

The experimental procedure followed during the research work is described in this section.

3.1.1 Preparation of specimen

- Three goat femural bone were purchased from the local butcher market.
- Then it was cleaned in the lab with surgical blades of number 11 and number 15, removing the flesh from outer surface.
- Then the epiphysis of bone were cut from both sides using hacksaw, as shown in Figure 3.1, and bone marrow was cleaned from inside, making it hollow. The lengths of the specimens were 100–110 mm.

Figure 3.1: Removal of epiphysis of bone.

- After cleaning and cutting, the bones were kept in a plastic frozen bag, to isolate from outside atmosphere. Bones were brought just one night before the experiment day, so that to use it as early as possible on next day, before any bone property changes happen. For precaution, surgical gloves were used.

3.1.2 ACRUB Setup

A schematic diagram of the machining setup is shown in Figure 3.2. The various components of the machining setup will be described briefly in this section.

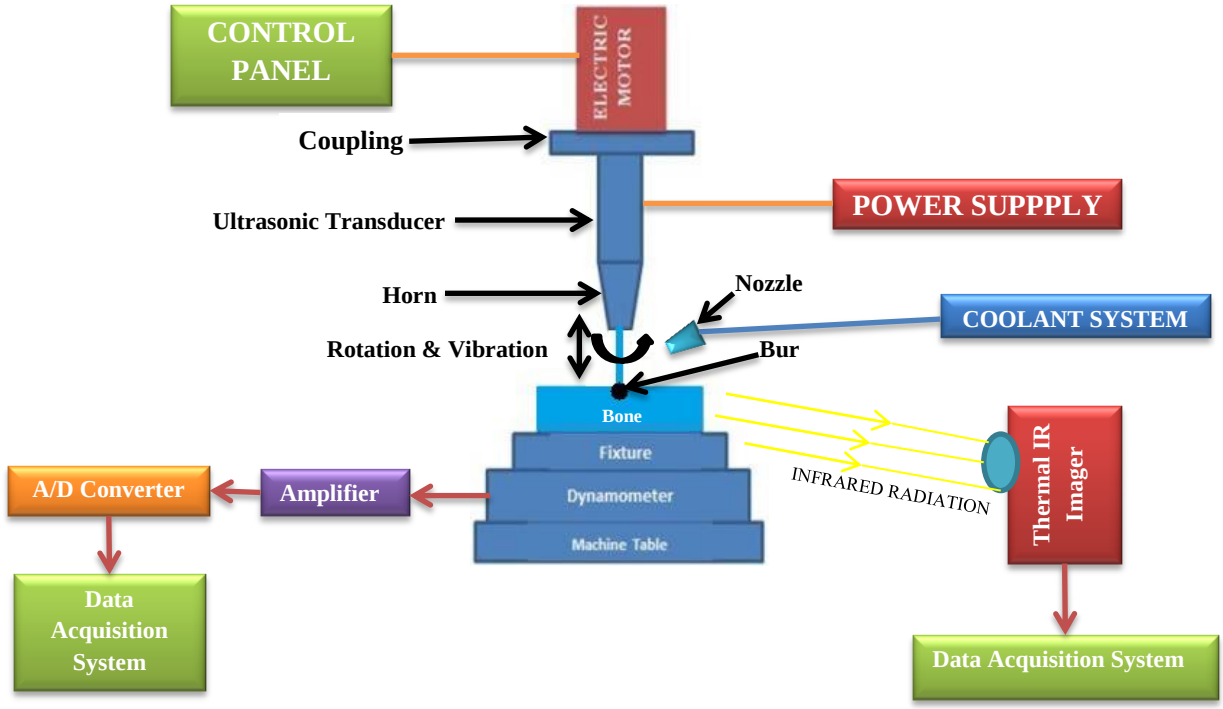

Figure 3.2: Schematic diagram of ACRUB

(i) **3-axis CNC vertical milling machine**- A CNC vertical milling machine (Make: BFW CHANDRA^{+}) was employed to give the tool three linear motions i.e. in x-direction, y-direction and z-direction. It has maximum range of 5000 rpm with feed rate lower range of 1 mm/min. As mentioned earlier, this is required to mimic the robotic system so that a precise control is maintained while machining. A piezoelectric transducer was fitted in the spindle system of machine, to give ultrasonic vibrations to the tool with amplitude 20 µm of frequency range 20,000 Hz to 25,000 Hz.

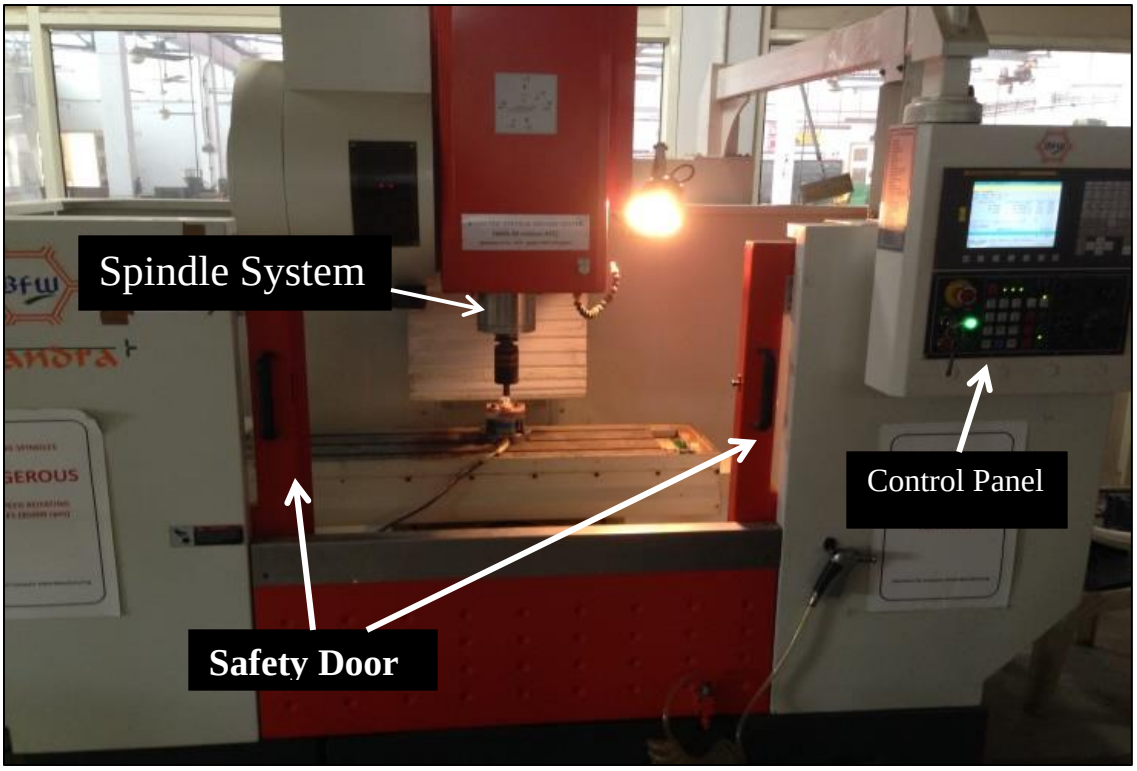

Figure 3.3: 3-axis vertical CNC milling center

Following CNC program was fed into the control panel to perform machining:

G90 G21; (G90= Absolute programming, G21= Metric units)

G00 X0 Y0 Z0; (Tool moves quickly using any random path to these coordinates)

G90 G54 S2000 F10; ('S' stands for Spindle Speed, 'F' stands for Feed Rate)

G01 Z-0.5; (Now command is given to tool to move depth of 0.5 mm)

G01 Y5; (Now tool is asked to move 5 mm horizontally in y-direction)

G01 Z1; (Now tool will move vertically in upward direction to reach 1 mm in positive z-direction)

M05; (Program Stop)

M30 (Program End)

(ii) **Tool**- A diamond round bur (Make: D+Z) was fitted in the collet in piezoelectric transducer. The tool is 70 mm in length, head diameter is 4 mm, and shank diameter is 2.35 mm. It is of medium sized grit tool with grain size varying from 105-120 µm (variation is due to their shape and size).

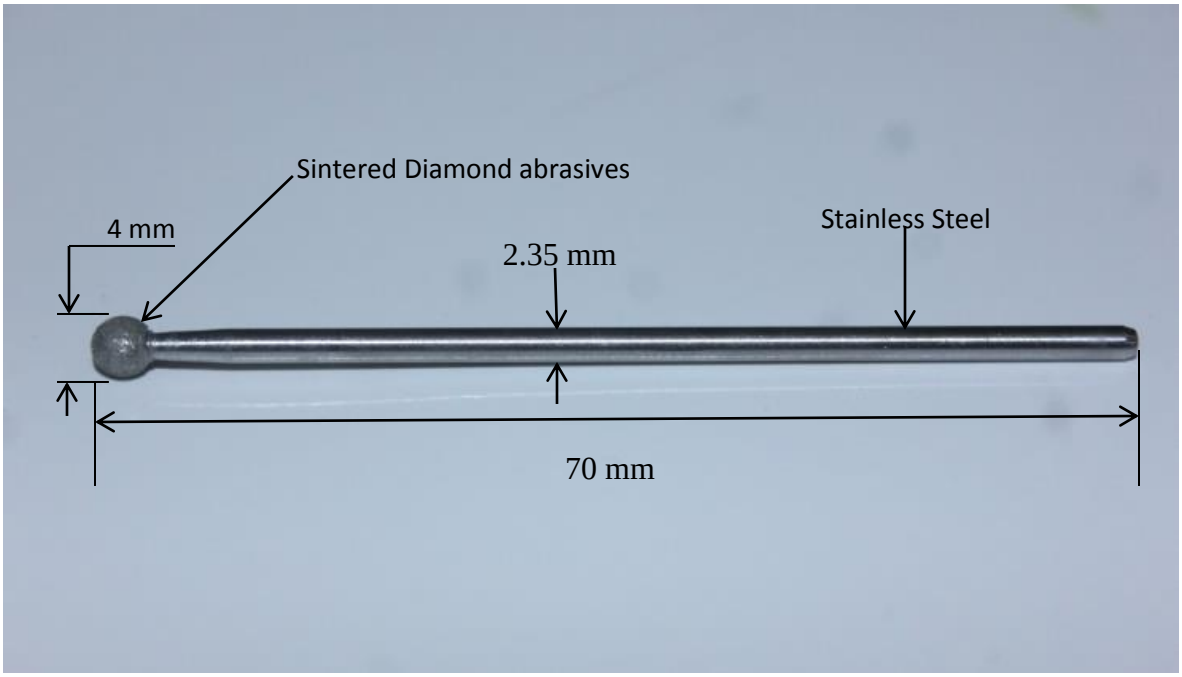

Figure 3.4: Diamond bur with grit size 90–120 FEPA.

This bur was selected subjected to its popularity in hospitals in India. Diamond burs are used for precision cutting and carbide burs are used where precision is not the case.

(iii) **Preparation of fixture**-

- A wooden board of dimension 100×100×20 mm was used as fixture to hold the specimen.
- Two holes of 8 mm in diameter were drilled with 7 cm spacing between them, as identical to holes of dynamometer.
- Then two C-type plastic clamps of 18 mm diameter, with holes to accommodate stainless steel screws of 38.1 mm in length, were hammered on it, with positioning shown in Figure 3.5.

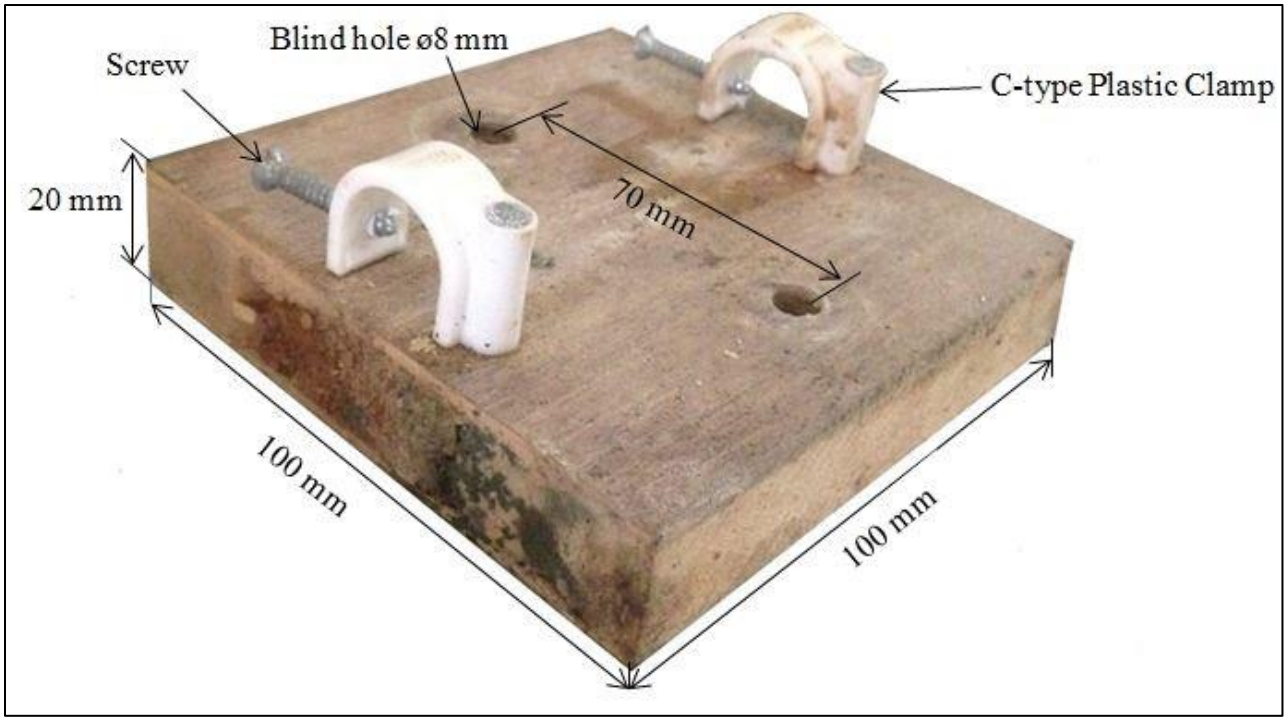

Figure 3.5: Wooden Fixture to hold the bone.

- The holes were also drilled in specimen to get hold up with screw. This fixture was then mounted on a piezoelectric dynamometer.
- The wooden fixture is light in weight.

(iv) **Coolant System-** Water was used as a coolant to cool the bone piece during burring and also, in removing and carrying the bone debris from the worked area.

(v) **Dynamometer-** A Kistler Dynamometer type 9272 is placed on bed of the CNC, above which the fixture stands, to measure the cutting force (F_z) of the bur. It is a piezoelectric type dynamometer. When force is applied, the piezoelectric sensor generates an output voltage which is received by the amplifier. The charge amplifier fed this signal to the computer system in which software, named as *Kistler Dynoware*, reads those signals and converts them to a force data with graphs.

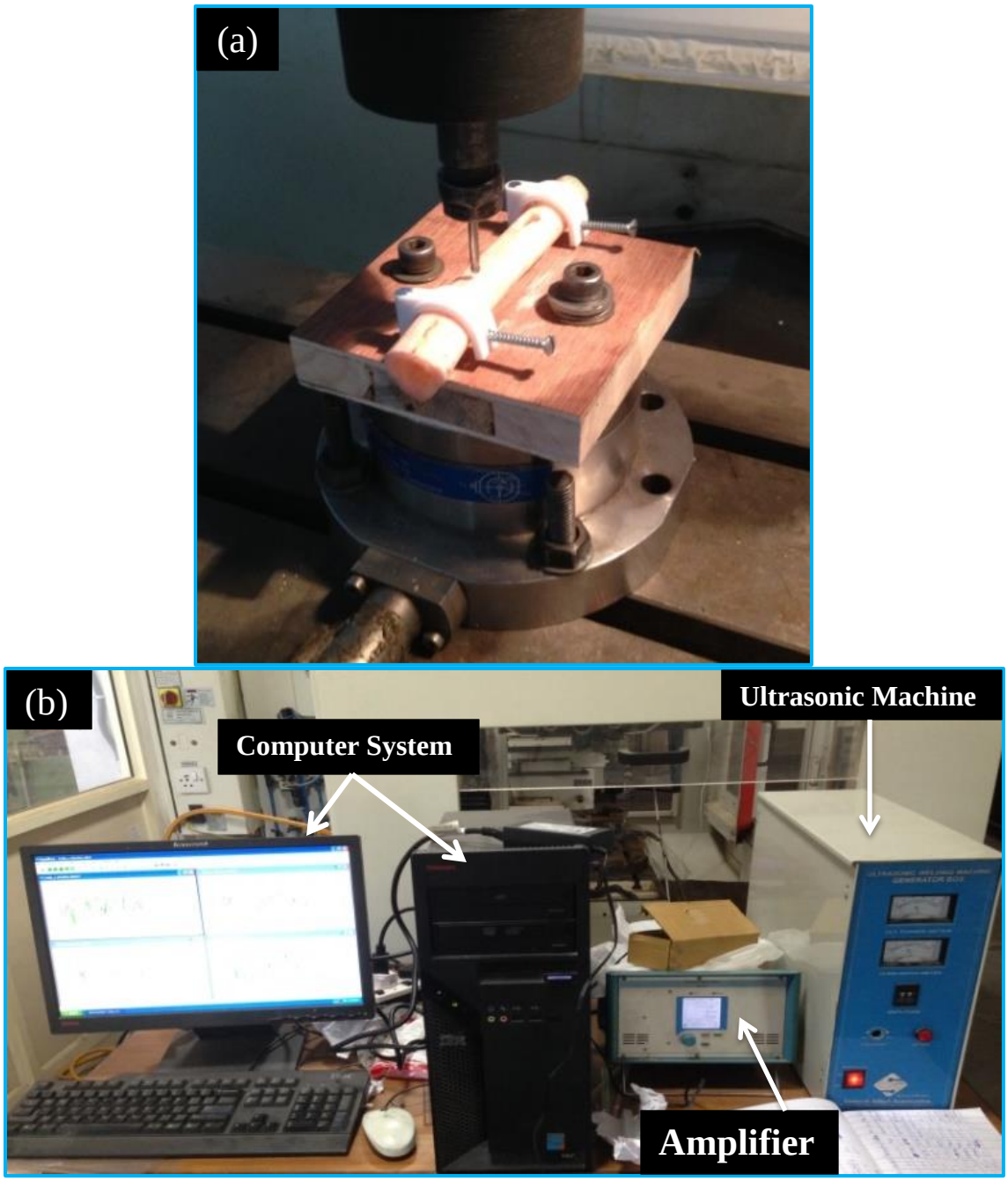

Figure 3.6: (a) A 9272 type Kistler Dynamometer holding fixture with (b) data acquisition system.

(vi) **Thermal IR Camera-** A U5855A TrueIR Thermal Imager (Manufactured by: Keysight Technologies) is used to take thermal images of the grinding operation. This model can measure up to 350°C with ability to focus on objects as close as 10 cm away. It comes with a fine resolution with 320 × 240 pixels. The camera can be used to make thermal videos with the help of *TrueIR Analysis and Reporting* tool. Due to this software, the

temperature graphs were easily achieved from videos. Figure 3.7 shows a typical thermal imager.

Figure 3.7: TrueIR Thermal Imager (Keysight Technologies).

After the fabrication of machine setup, it was run to check its workability and performance with various process parameters on a wooden material. There are various process parameters for burring of bone. The input process parameters have been judicially selected on the basis of literature reviews, are shown in Table 3.1.

Table 3.1 Input process parameters

Parameters / Levels	Parameter(A) *Spindle Speed (rpm)*	Parameter(B) *Feed Rate (mm/min)*	Parameter(C) *Depth of cut (mm)*
1	3000	1	0.5
2	4000	1.5	0.75
3	5000	2	1

3.1.3 Design of experiment

Design of experiments (DOE) is a technique which decides in a standard way, the relationship between variables influencing a procedure and its results. The utilization of this method is to discover the set of conditions and connection of end results. To manage the input parameters for optimization is the expectation from the data.

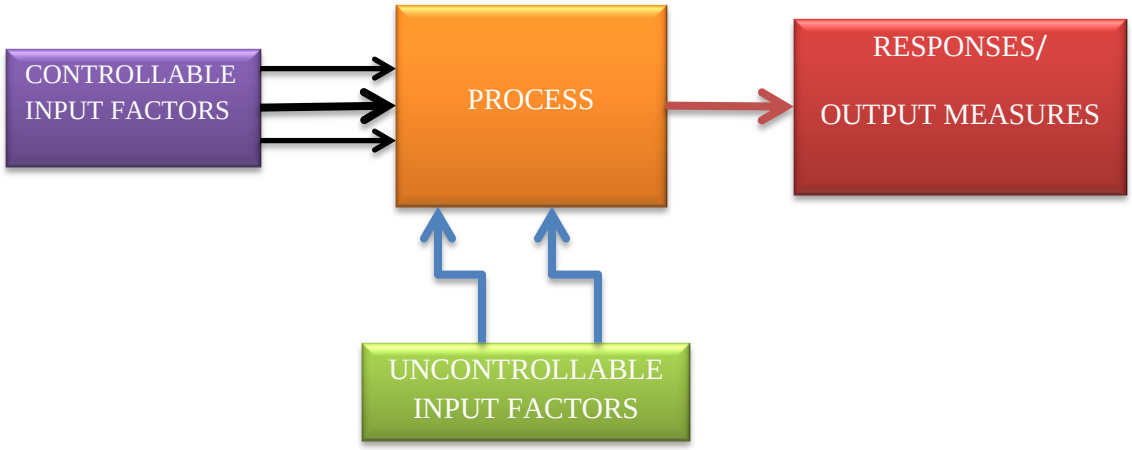

Figure 3.8: Concept of DOE

❖ Approaches to DOE

- Response surface methodology
- Fractional factorial approach
- Full factorial approach
- Mixture experiments
- Taguchi methods

This study deals with Taguchi methods. A Japanese analyst “Genichi Taguchi” introduced this experimental design, which makes analysis methodically by exploring the relationship between the levels of element selected and outputs driven from that design test. The technique is applied to check the process execution and its accuracy. It is effective in reducing the factors involved in process, so that study is effective without affecting its accuracy.

Regularly used orthogonal arrays of Taguchi DOE are as follows:

- L-9
- L-18

- L-27
- L-36

In this thesis work, a total of three studies have been conducted. First, L-9 orthogonal array has been applied only for dry conventional grinding (DCG) i.e. a total of nine set of experiments have been performed. The optimum parameters are obtained. Then on finding the experiment with best result in L9 experiment set from DCG, the parameters were tested with dry (ACRUB + CG); and finally, ACRUB with cooling system. For DCG, the ACRUB setup is used, as ultrasonic machine was not employed.

Input parameters and control log of experimentations:

The input process parameters have been selected as per literature reviews. The complete control log and DOE is presented in Table 3.2.

Table 3.2 Control log experimentation and process parameter.

EXPERIMENT NO.	Parameter(A) *Spindle Speed, s (rpm)*	Parameter(B) *Feed Rate, f (mm/min)*	Parameter(C) *Depth of cut, d (mm)*
1	3000	1	0.5
2	3000	1.5	0.75
3	3000	2	1
4	4000	1	0.75
5	4000	1.5	1
6	4000	2	0.5
7	5000	1	1
8	5000	1.5	0.5
9	5000	2	0.75

A total of 3 bones, as prepared, were used for study. The cutting length of 5 mm was made using the bur (in second study, 2.5 mm for dry ACRUB then next 2.5 mm for dry conventional grinding).

The controllable factors are spindle speed, feed rate and depth of cut, though there are other parameters like grit size, amplitude, frequency, head diameter, etc, but kept constant throughout the experimentation. There are further three levels of each selected factor in the DCG study, as in case of spindle speed the machine was run at 3000 rpm, 4000 rpm, and then 5000 rpm (which

can be changed using CNC machine control panel). Whereas for feed rate and depth of cut three different ranges were selected as 1 mm/min, 1.5 mm/min, 2 mm/min and 0.5, 0.75, and 1 mm respectively. For each of experiment in DCG study three trials were performed. Some of the specimens burred in each of these studies using different controllable factors are shown in Figure 3.9.

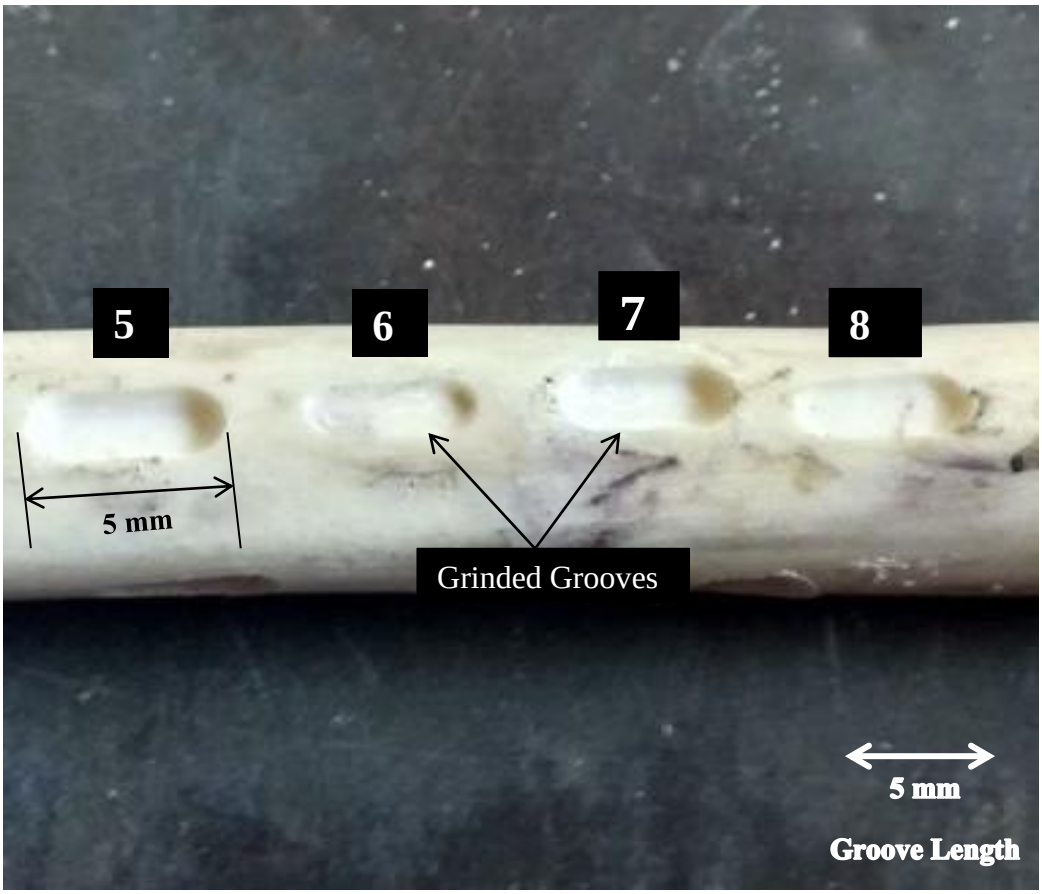

Figure 3.9: Bone specimen grinded using DCG. (5, 6, 7 and 8 represents experiment number)

The output parameters were then selected on the basis of literature review and issues in surgery.

- Selected output parameters:
  - Thermal analysis
  - Normal Force (F_Z)

3.5.4 Experimental Procedure

As discussed earlier, a 5 mm (half ACRUB and half conventional grinding in second case) cut is made on bone using diamond round bur with the parameters decided from DOE. Simultaneously, temperature of tool-bone interface and normal cutting force exerted on bone, were recorded using thermal imager and dynamometer, respectively. Table 3.3 contains constant parameters used during the grinding procedure.

Table 3.3 Constant parameter.

Length of cut	5 mm
Amplitude	20 µm
Frequency range	20,000 Hz – 25,000 Hz
Diameter of bur	4 mm

Thermal Analysis:

Thermal necrosis is one of the major constraints during surgical operations with conventional techniques. To check temperature, a thermal IR camera has been used. Table 3.4 is the parameter settings in Thermal camera.

Table 3.4 Thermal IR camera parameter setting.

Emissivity, ε	0.98 (Human Skin)
Reflected Temperature	25.1 °C
Ambient Temperature	25 °C
Distance	1 m
Humidity	50 %
Temperature Range	0 – 350 °C
Record Interval	0.125 sec
Frames per sec	8 fps

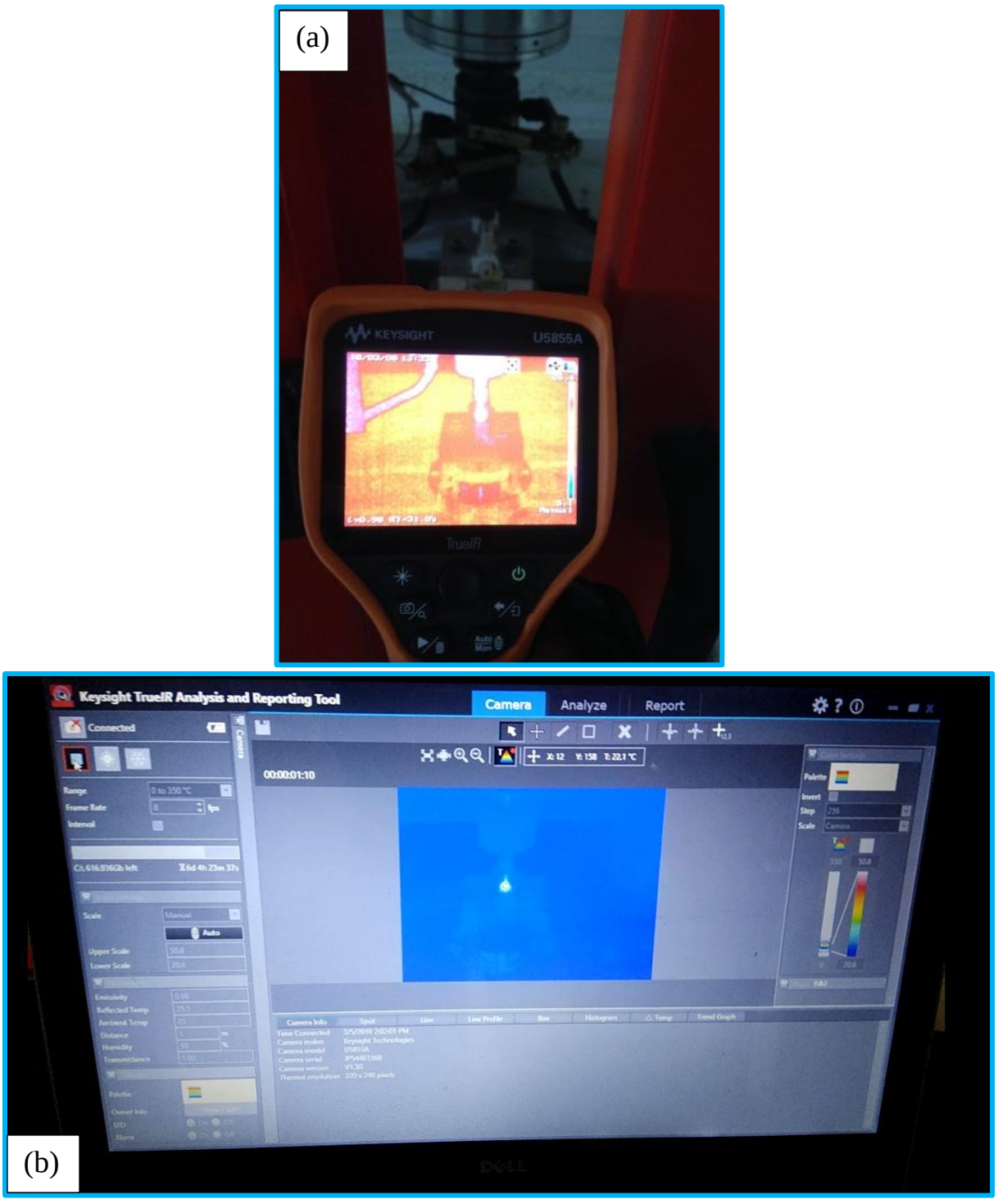

Figure 3.10: (a) Working of thermal imager (Make: Keysight Technologies) and (b) Working of TrueIR analysis and reporting software.

In this thesis work for thermal analysis *TrueIR Analysis and Reporting Tool* software, shown in Figure 3.10 (b), has been used along with IR camera. Through software the temperature readings and trend graph between instant temperatures and machining time was obtained in excel format.

The average temperature readings of three trials in each of the experiment in dry conventional grinding have been displayed in Table 3.5.

Table 3.5 Average temperature (°C) at the point of tool and work interface in case of DCG of individual experiments.

Experimentation run no.↓	*Average dry conventional grinding temperature (°C)*
1	39.6729
2	67.6768
3	84.0717
4	60.6293
5	74.6385
6	42.8954
7	55.3426
8	34.3168
9	55.1807

Normal Force Analysis:

Along with the temperature, it is also important to keep a check on Normal Force(F_Z). So, the normal force was measured with the help of a Piezoelectric-type Dynamometer, to compare the three cases, and prove that ACRUB is a superior process to conventional-type of surgery. Table 3.6 shows the average force calculated by mean of forces measured in three trials of each trial.

Table 3.6 Average normal forces (N) in conducted nine experiments in dry conventional grinding.

Experimentation run no.↓	*Average dry conventional grinding force (N)*
1	1.898
2	2.768
3	3.716
4	2.276
5	2.937
6	2.018
7	2.062
8	1.532
9	2.106

Microstructure Evaluation equipment:

SEM set-up (JSM 6510 LV, JEOL Ltd., Tokyo, Japan) was used to study the surface topography produced after grinding in three different cases. Samples were cut out from the specimen to fit four samples at a time on the scanning plate and aid in scanning rate. The maximum specimen upto 150 mm diameter could be accommodated and magnification varied from 30 X–1,00,000 X. The bone samples were first coated with gold in an Auto Fine Coater (JFC-1600, JEOL Ltd., Tokyo, Japan), and then it was fed into the machine for analysis.

Figure 3.11: Auto Fine Coater used for coating the bone specimens.

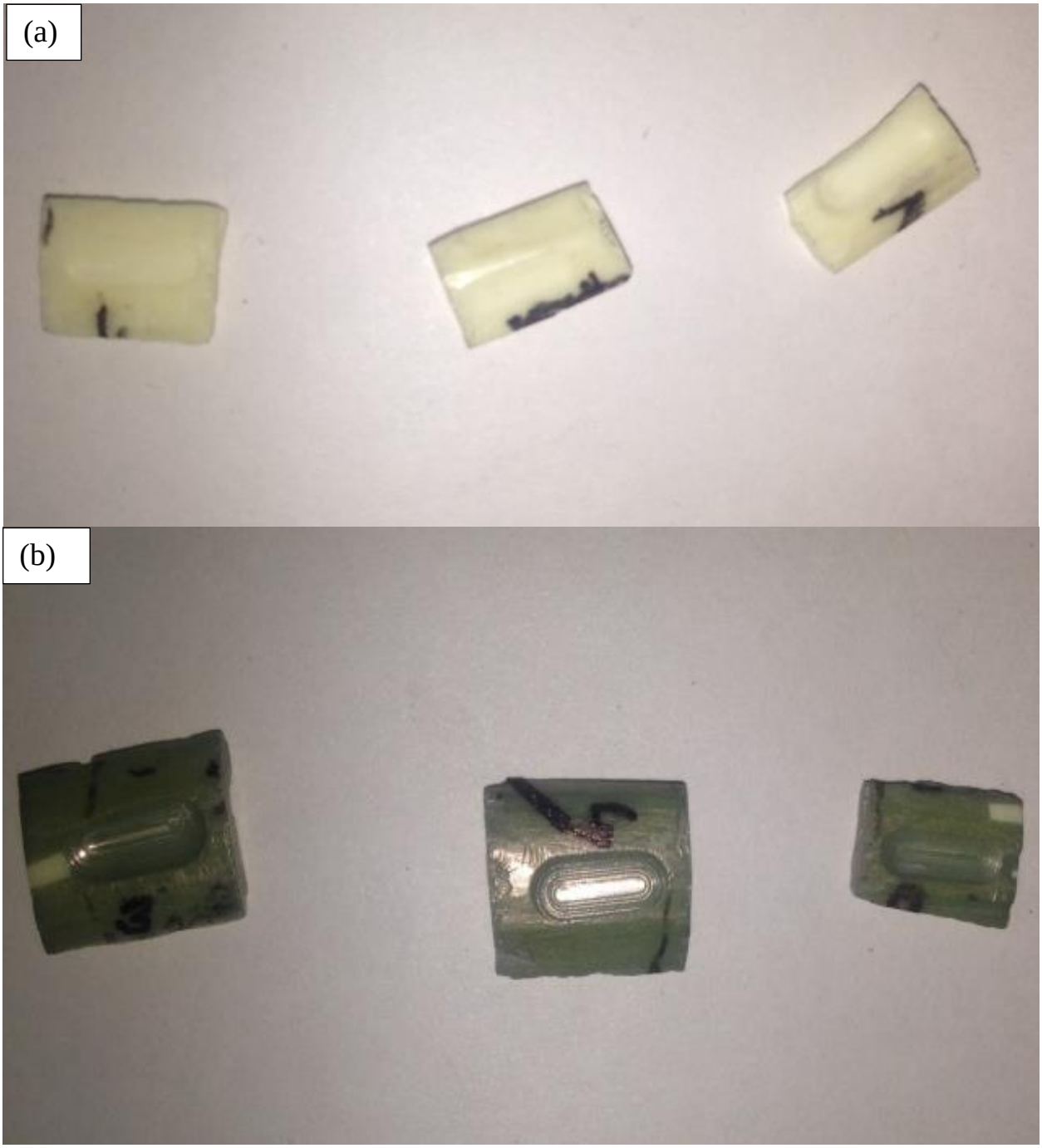

Figure 3.12: (a) Some samples cut out from single bone and (b) Samples after coating.

Figure 3.13: SEM set-up used for microstructural characterization in the present work.

3.2 Summary of the chapter

In this chapter, the objective of the present research work and the key issues to be taken up during the work were discussed. The experimental procedure followed during research work and the procedure to prepare bone specimens were discussed in detail. Furthermore, the equipment used for grinding/burring of samples, temperature measurement, force measurement and microstructure evaluation was discussed.

Chapter 4
Results and Discussion

4 Results and Discussion

4.1 Dry conventional grinding

In dry conventional grinding (DCG), the bur first moves vertically downward at feed rate, then it is made to traverse at same feed rate horizontally up to 5 mm length, and then it is traversed vertically upwards to reach positive position Z1.

4.1.1 Thermal Analysis

From Table 3.5 it was observed that the lowest average temperature (34.3168°C) was recorded in experiment 8 and highest average temperature (84.0717°C) in experiment 3 in case of dry conventional grinding. The reason is that higher the spindle speed lower will be the temperature, and lower the feed rate and spindle speed, lower will be the temperature [15, 18, and 19]. Considering the parameters it is understood that experiment 8 happens to be the case of low temperature. Figures 4.1 and 4.2 illustrate graphs of temperature measurement versus frame for experiments 8 and 3, respectively, measured through thermal imager at 8 fps. It may be observed from Figure 4.1 that there are three distinct zones: Zone-1, Zone-2, and Zone-3 i.e. when bur moving vertically downwards, horizontal, and again moving vertically upwards, respectively. From literature it was observed that the threshold temperature for necrosis varied from 43°C to 51°C [15, 16, 18, 19, 20, 21 and 30]. For this experiment, it was decided to consider the minimum value of necrosis, 43°C as shown in Figures 4.1 and 4.2.

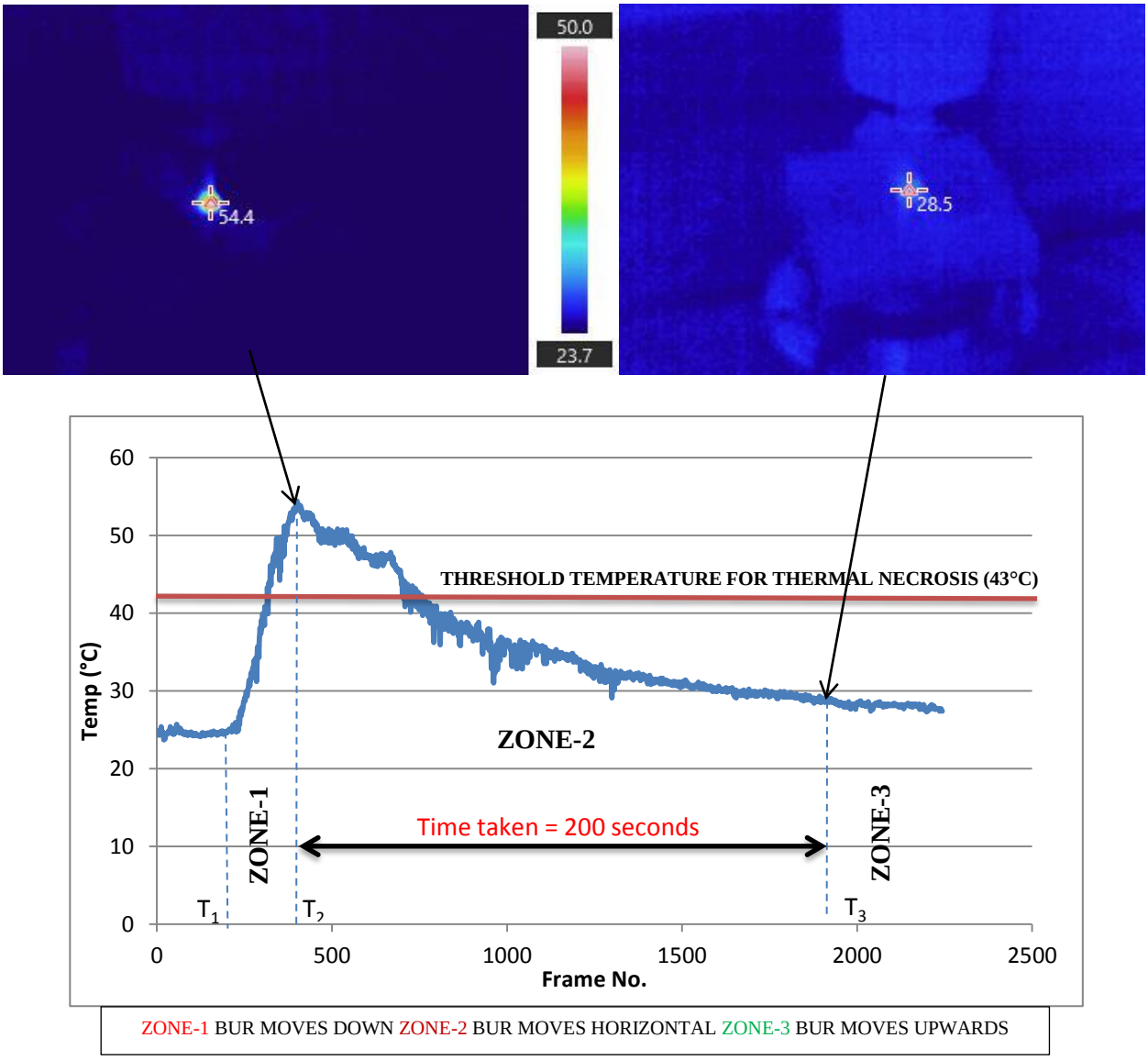

Figure 4.1: Temperature graph at s= 5000 rpm, f= 1.5 mm/min and d= 0.5 mm with thermal images.

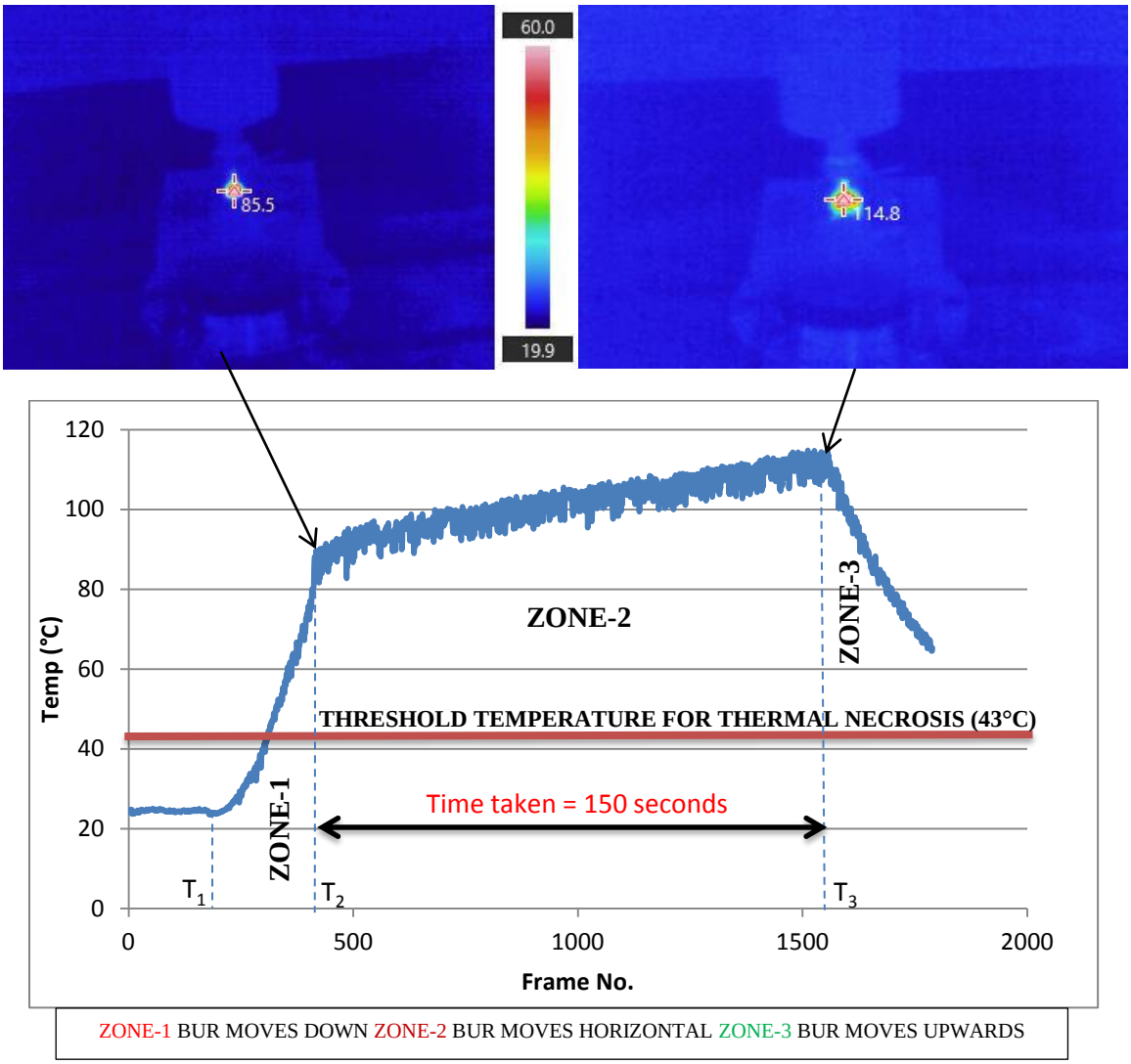

Figure 4.2: Temperature graph at s= 3000 rpm, f= 2.0 mm/min and d= 1 mm with thermal images.

In Figure 4.1, at temperature T_1, the grinding process starts as this is the point where bur makes contact with the bone. There is sharp rise in temperature which is due to bur traversing vertically downwards and there is poor heat loss to surroundings due to very low conductivity of bone and giving no way to bone debris, leaving only medium of heat conduction i.e. through bur leading sharp rise to temperature T_2 (Figure 4.3 (a)). This temperature is the point where bur has finished corresponding depth of cut. After this point, there is decrease in temperature till T_3 because the bur is now travelling in horizontal direction due to which the area of contact between bur-bone has been reduced to half, as shown in Figure 4.3 (b), resulting in non-contact area open to atmosphere and thus, leading to conduction of heat to air. Then at temperature T_3, there is decrease in sharp decrease because the bur is now traversing vertically upwards, due to which there is no contact between the bur and bone surface and it takes time to cool down. There is some temperature due to contact of bur with the debris. The graph here is for machining time only.

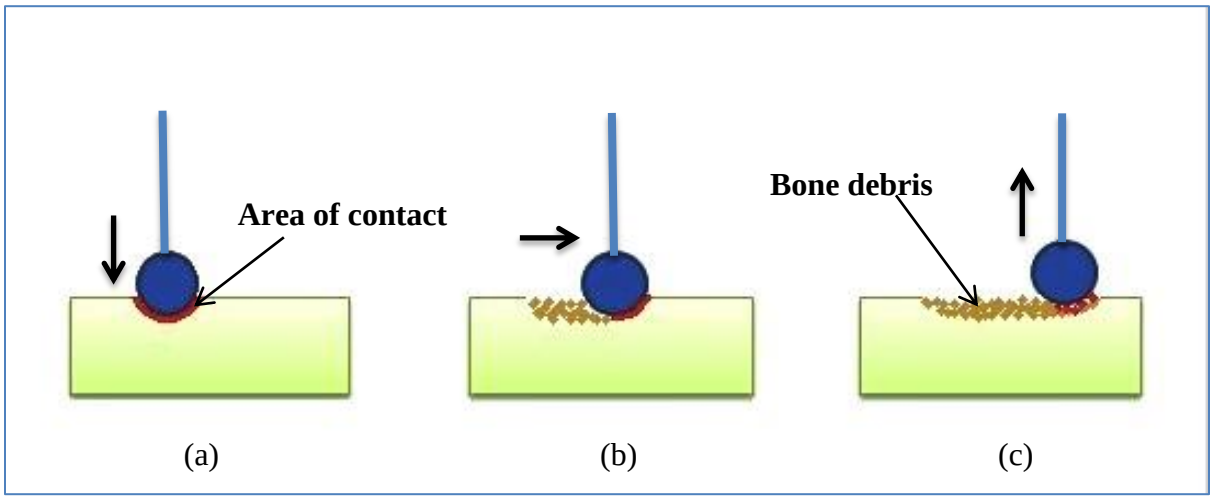

Figure 4.3: (a) Downward motion of bur, (b) Horizontal motion of bur, and (c) Upward motion of bur.

Similarly, in Figure 4.2, the reasons for temperature rise and fall in Zone-1 and Zone-3 are the same. But in Zone-2, the temperature is still increasing at low slope as compared to previous Zone-1 because it may be that the bone surface to which the bur made contact was taper at some angle, due to some deformities in bone, and 1mm depth of cut added more area of contact as compared to experiment8 leading to increase in thermal energy and additionally, the feed-rate was higher as compared to experiment 8, thus, aiding in increase in temperature. Also, it is

evident from observations that all the experiments violate the limit of thermal necrosis temperature of 43°C.

The average temperatures, $T_{avg,}$ calculated have been further optimized using MINITAB 17 software. The experimental control log average values and S/N ratios are shown in Table 4.1.

Table 4.1 Control log and S/N ratios for thermal analysis of dry conventional grinding

EXPERIMENT NO.	Parameter(A) *Spindle Speed (rpm)*	Parameter(B) *Feed Rate (mm/min)*	Parameter(C) *Depth of cut (mm)*	Average Temperature *(°C)*	S/N Values (*db*)
1	3000	1	0.5	39.6729	-31.9699
2	3000	1.5	0.75	67.6768	-36.6088
3	3000	2	1	84.0717	-38.4930
4	4000	1	0.75	60.6293	-35.6536
5	4000	1.5	1	74.6385	-37.4593
6	4000	2	0.5	42.8954	-32.6482
7	5000	1	1	55.3426	-34.8612
8	5000	1.5	0.5	34.3168	-30.7101
9	5000	2	0.75	55.1807	-34.8357

To evaluate the effect of selected input factors on the measured output parameters has been evaluated with the Analysis of Variance. The S/N ratio plot for $T_{avg,}$ (see Table 4.1) at smaller the better has been analyzed.

For smallest the better, formula used was: $-10 \times \log_{10}\left(\frac{\sum y^2}{n}\right)$ (4.1)

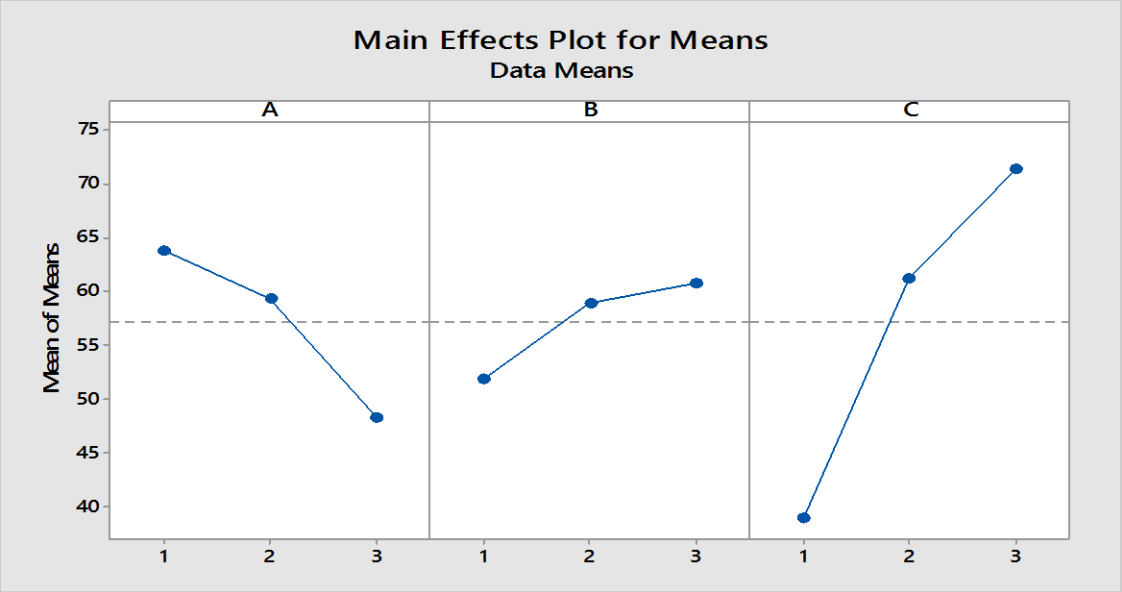

Figure 4.4: Mean graph for average temperatures.

The mean graph shown in Figure 4.3 was obtained for smaller the better type case, the graph suggests that with increase in spindle speed the average temperature of the bur-bone interface has decreased. This is because when spindle speed is increased the brittle to ductile transition takes place on bone surface and material removal is easier, and thus temperature is lower at higher spindle speeds. In case of the feed-rate the average temperature increases with increase in feed-rate. This is because with increase in feed-rate the force acting increases, which increases the frictional forces and gives less time to the bone debris to flush out which aids in frictional force , thus, increasing thermal energy. The depth of cut, d, has majorly affected on the temperature of the specimen. Higher the depth of cut, higher will be the temperature, because on increase in d, the area of contact between bur-bone increases and thus, the resistive force of the diamond bur will increase leading to increase in frictional heat.

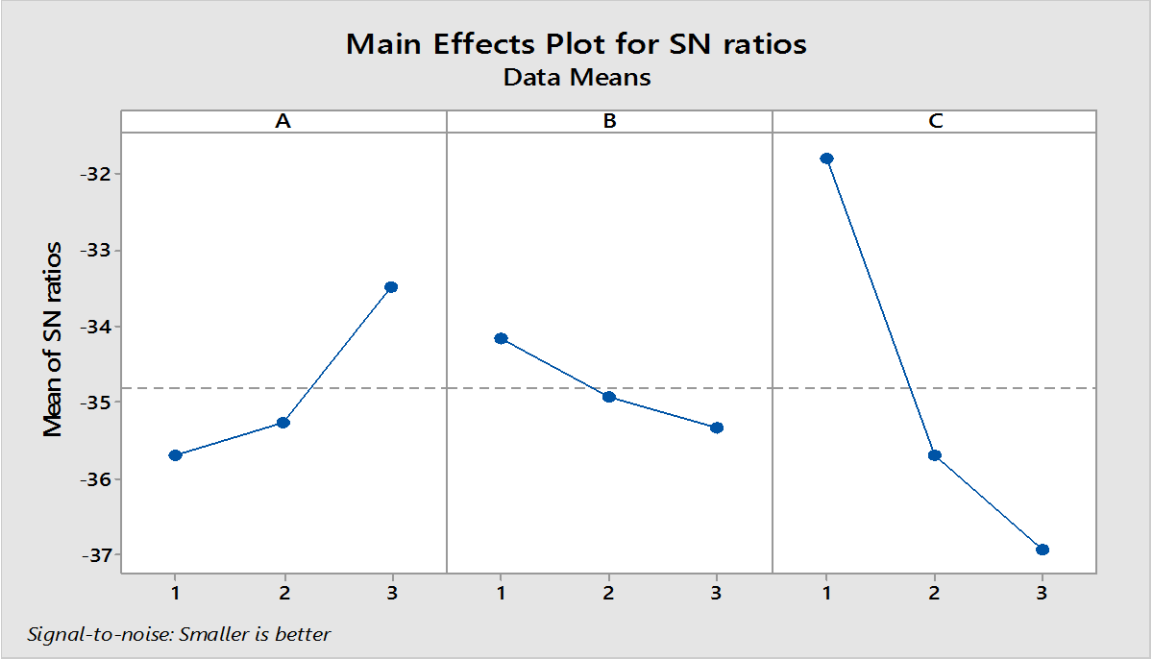

Figure 4.5: S/N graph for average temperatures $T_{avg.}$

As higher the S/N ratio better will be the required result, so, in smaller the better type case, the optimum parameters with least value of T_{avg} were combination (A3B1C1).

Analysis of variance (ANOVA) for S/N ratios has shown the percentage contribution of each input parameter towards average temperature of the grinded specimens (see Table 4.2). Table shows that all the three parameters are significant due to their 'p' value less than 0.05 and depth of cut has greater contribution to increase the temperature.

Table 4.2 Analysis of Variance for SN ratios for average temperature

Factor	DoF	Seq. SS	Adj SS	Adj MS	F	P	%age Contribution
A	2	8.3111	8.3111	4.1556	81.54	0.012	15.37
B	2	2.0992	2.0992	1.0496	20.59	0.046	3.88
C	2	43.5697	43.5697	21.7849	427.45	0.002	80.56
Residual Error	2	0.1019	0.1019	0.0510			0.188
Total	8	54.0820					

DoF- Degree of freedom; Seq. S.S- Sum of squares; Adj S.S- Adjacent sum of squares; F value- Fishers value; P value - Probability

The response table for S-N ratios at smaller the better type case (Table 4.3) suggests that depth of cut, *d*, has major effect on the average temperature of the bur-bone interface. Then spindle speed, *s*, and then feed-rate, *f*, with least effect.

Table 4.3 Response Table for S-N Ratio for average temperature (smaller the better)

Levels	A	B	C
1	-35.69	-34.16	-31.78
2	-35.25	-34.93	-35.70
3	-33.47	-35.33	-36.94
Delta	2.22	1.16	5.16
Rank	2	3	1

4.1.2 Normal Force Analysis

From Table 3.6, it was observed that lowest average normal force was recorded at experiment 8 (1.53248 N) and highest average force at experiment 3 (3.71 N). Figures 4.6 and 4.7, illustrates graphs of force measured versus time for experiments 8 and 3, respectively, measured by Dynamometer. As higher the spindle speed, lower will be the force and when lower the feed rate and depth of cut, lower will be the force [31]. Considering the parameters, the experiment 8 will give low normal force as compared to other experiments. It may be observed from Figure 4.6 that when bur starts cutting vertically downwards, the normal force (F_Z) starts increasing and reaches 7.629 N at 17^{th} sec, where it finishes the 0.5 mm depth of cut, because the bur does not let the bone debris to escape easily resulting in exertion of force on the bur (Figure 4.3 (a)). Then there is a decrease in normal force due to movement of bur in horizontal direction till 217^{th} sec, where it completes the length of cut 5 mm, because of escaping of bone debris to the free side of the bur the pressure of bone debris is reduced (Figure 4.3 (b)). Then there is drop in force level due to movement of bur vertically upwards. There is still some normal force due to presence of some bone debris in small gap which exerts force on bur, and then after some time it finally diminishes.

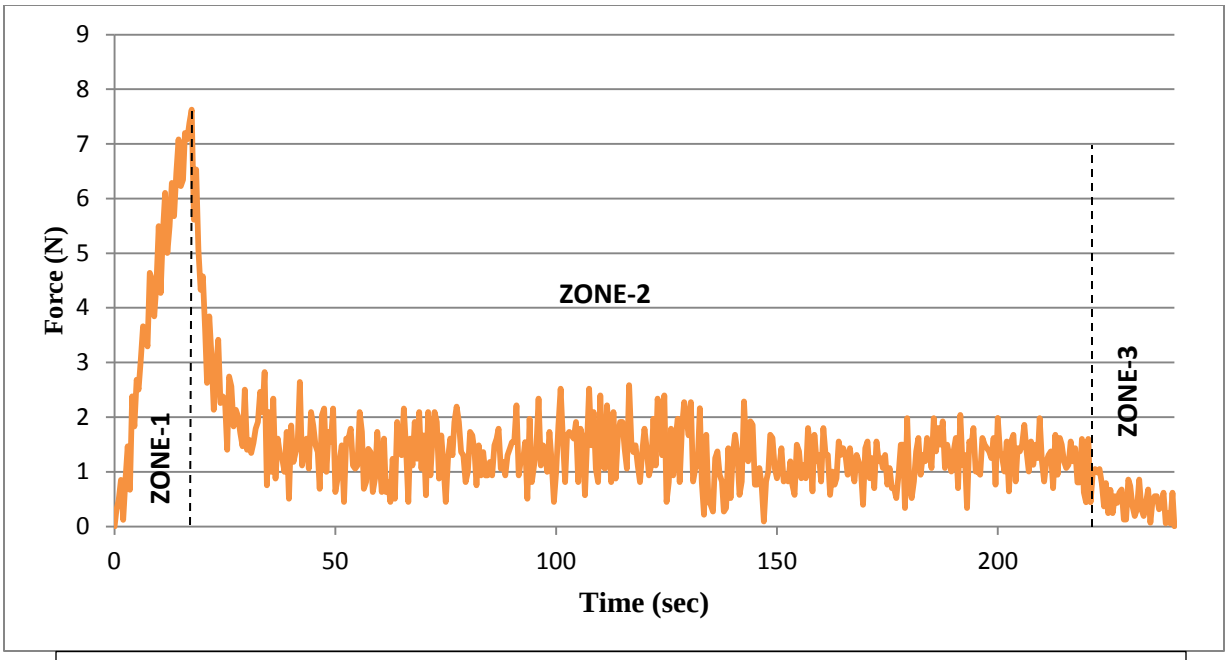

ZONE-1 BUR MOVES DOWN ZONE-2 BUR MOVES HORIZONTAL ZONE-3 BUR MOVES UPWARDS

Figure 4.6: Force versus time graph at s= 5000 rpm, f= 1.5 mm/min and d= 0.5 mm

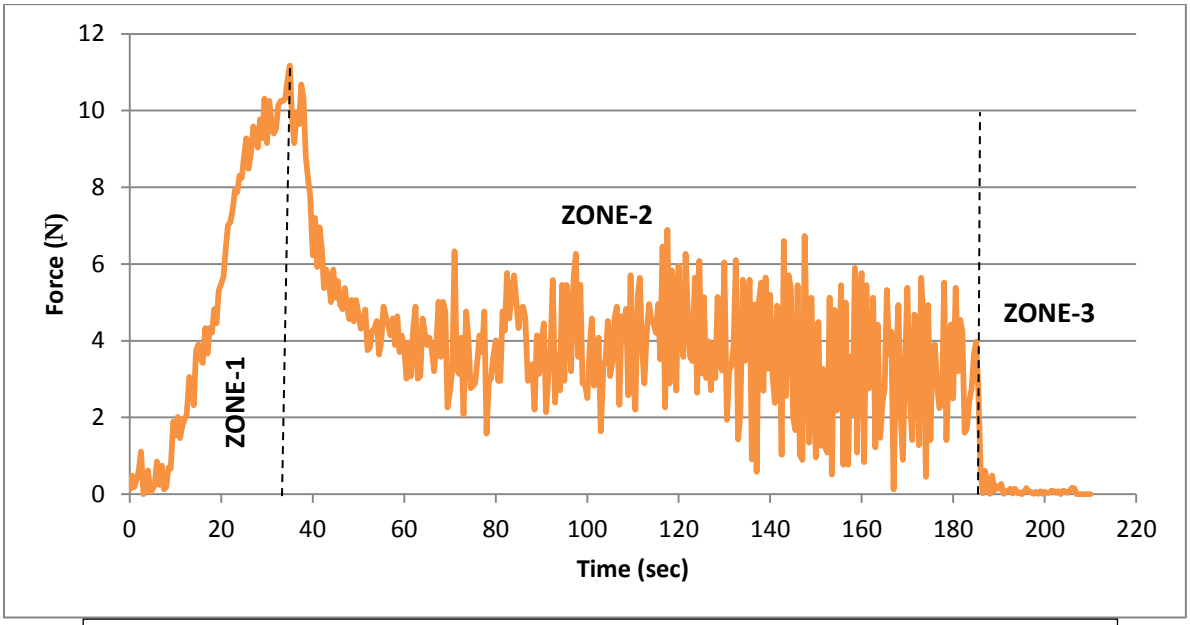

ZONE-1 BUR MOVES DOWN ZONE-2 BUR MOVES HORIZONTAL ZONE-3 BUR MOVES UPWARDS

Figure 4.7: Force versus time graph at s= 3000 rpm, f= 2.0 mm/min and d= 1 mm

Similarly, in Figure 4.7 the force reaches its peak at 11.1694 N at 35th sec where bur completes 1 mm depth of cut moving vertically, then there is decrease in force, reaching at average force of about 3.8 N because bur is moving horizontally due to which area of contact is half as compared to coming downwards and this leads to escape of bone debris releasing the pressure on bur. At 185th sec the bur starts leaving the surface at feed rate 2 mm/min leading to reduction in normal force, with still some force exerted by bone debris left under the bur.

The average forces, F_{ZAvg} calculated have been further optimized using MINITAB 17 software. The experimental control log average values and S/N ratios are shown in Table 4.4.

Table 4.4 Control log and S/N ratios for normal force analysis.

EXPERIMENT NO.	Parameter(A) *Spindle Speed (rpm)*	Parameter(B) *Feed Rate (mm/min)*	Parameter(C) *Depth of cut (mm)*	Average Normal Force *(F_Z)*	S/N Values (*db*)
1	3000	1	0.5	1.89841	-5.5678
2	3000	1.5	0.75	2.76804	-8.8435
3	3000	2	1	3.71648	-11.4026
4	4000	1	0.75	2.27627	-7.1445
5	4000	1.5	1	2.93687	-9.3577
6	4000	2	0.5	2.01805	-6.0986
7	5000	1	1	2.06247	-6.2877
8	5000	1.5	0.5	1.53248	-3.7079
9	5000	2	0.75	2.10579	-6.4683

To evaluate the effect of selected input factors on the measured normal forces, parameters have been evaluated with the Analysis of Variance. The mean graph (Figure 4.8) and S/N ratio plot for F_{ZAvg} (see Table 4.4) at smaller the better has been analyzed. In smaller the better type case, the optimum parameters having least value of F_{ZAvg} was considered best as compared to others i.e. combination (A3B1C1). In L9 experiment set lowest normal force was observed in experiment 8. To calculate S/N values, Equation 4.1 was used.

Figure 4.8: Mean graph for normal force values.

The mean graph shown in Figure 4.8 was obtained for smaller the better type case, the graph suggests that with increase in spindle speed the average force of the bur-bone interface has decreased. This is because when spindle speed is increased the Brittle-to- Ductile transition takes place on bone surface and material removal is easier, and thus normal force is lower at higher spindle speeds. In case of the feed-rate the average normal force increases with increase in feed-rate. This is because with increase in feed-rate the force acting increases, which increases the pressure on bur and gives less time to the bone debris to escape out which aids in building more pressure on bur, thus, increasing mechanical energy. The depth of cut, *d*, has majorly affected on the average force of the specimen. Higher the depth of cut, higher will be the force, because on increase in *d*, more bone chips will be produced and thus, the resistive force of the diamond bur will increase leading to increase in pressure buildup as compared to others.

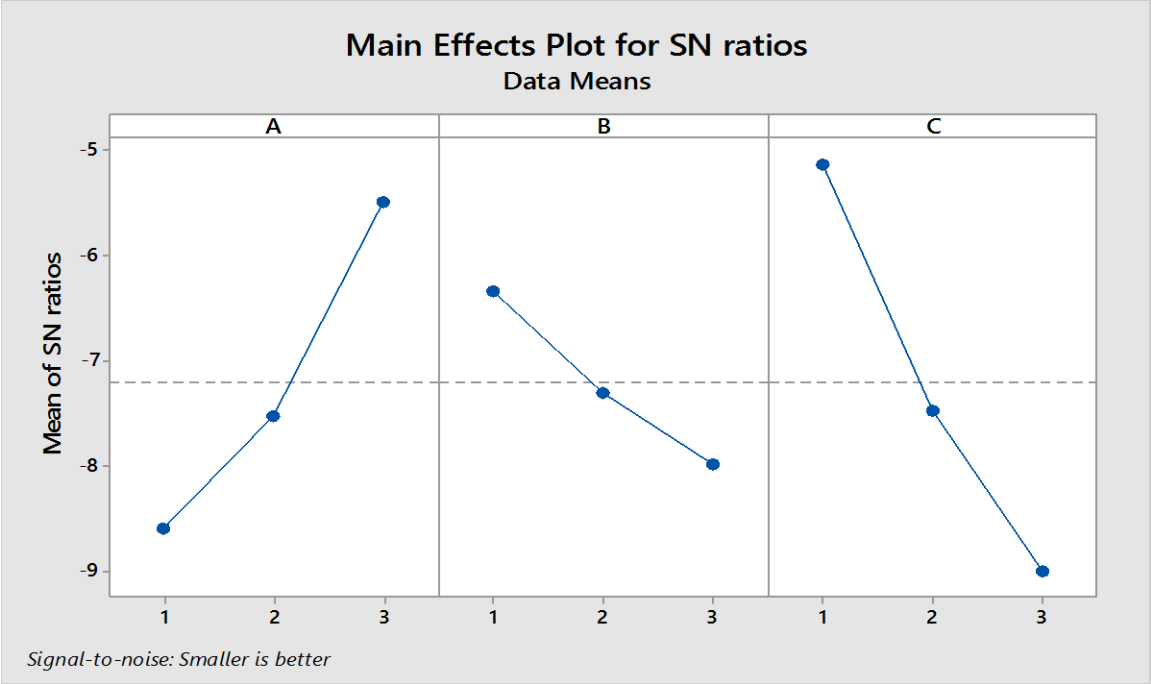

Figure 4.9 S/N responses to normal force values

As higher the S/N value, best will be the parameter, so it is found that the parameters combination with high S/N value is A3B1C1.

Analysis of variance (ANOVA) for S/N ratios has been performed at 95 % confidence level to obtain the percentage contribution of each input parameter towards average normal force of the grinded specimens (see Table 4.5). Table shows that all the three parameters are significant due to their 'p' value less than 0.05 and depth of cut has greater contribution to increase the normal force.

Table 4.5 Analysis of Variance for SN ratios for average normal force

Factor	DoF	Seq. SS	Adj SS	Adj MS	F	P	%age Contribution
A	2	15.0451	15.0451	7.5226	74.42	0.013	35.43
B	2	4.1561	4.1561	2.0780	20.56	0.046	9.79
C	2	23.0572	23.0572	11.5286	114.05	0.009	54.30
Residual Error	2	0.2022	0.2022	0.1011			0.476
Total	8	42.4605					

Table 4.6 shows response table for S-N ratios at smaller the better type, it suggests that depth of cut, *d*, has maximum contribution and feed-rate, *f*, has minimum effect on F_{ZAvg}.

Table 4.6 Response table for S/N values at smaller the better condition

Levels	A	B	C
1	-8.605	-6.333	-5.125
2	-7.534	-7.303	-7.485
3	-5.488	-7.990	-9.016
Delta	3.117	1.657	3.891
Rank	2	3	1

4.1.3 SEM Analysis

As explained in chapter 3, in scanning electron microscope the electrons beam are focused on sample to scan the surface, thus producing images and gives surface topography information and the composition of the sample.

After successful runs of thermal analysis and normal force analysis, the specimens with best and worst result have been used for microscopic analysis. As told earlier, for good conductivity samples were coated with a very fine layer of gold with automatic fine coater machine. SEM analysis was conducted on bone specimens to examine the surface of the burred area.

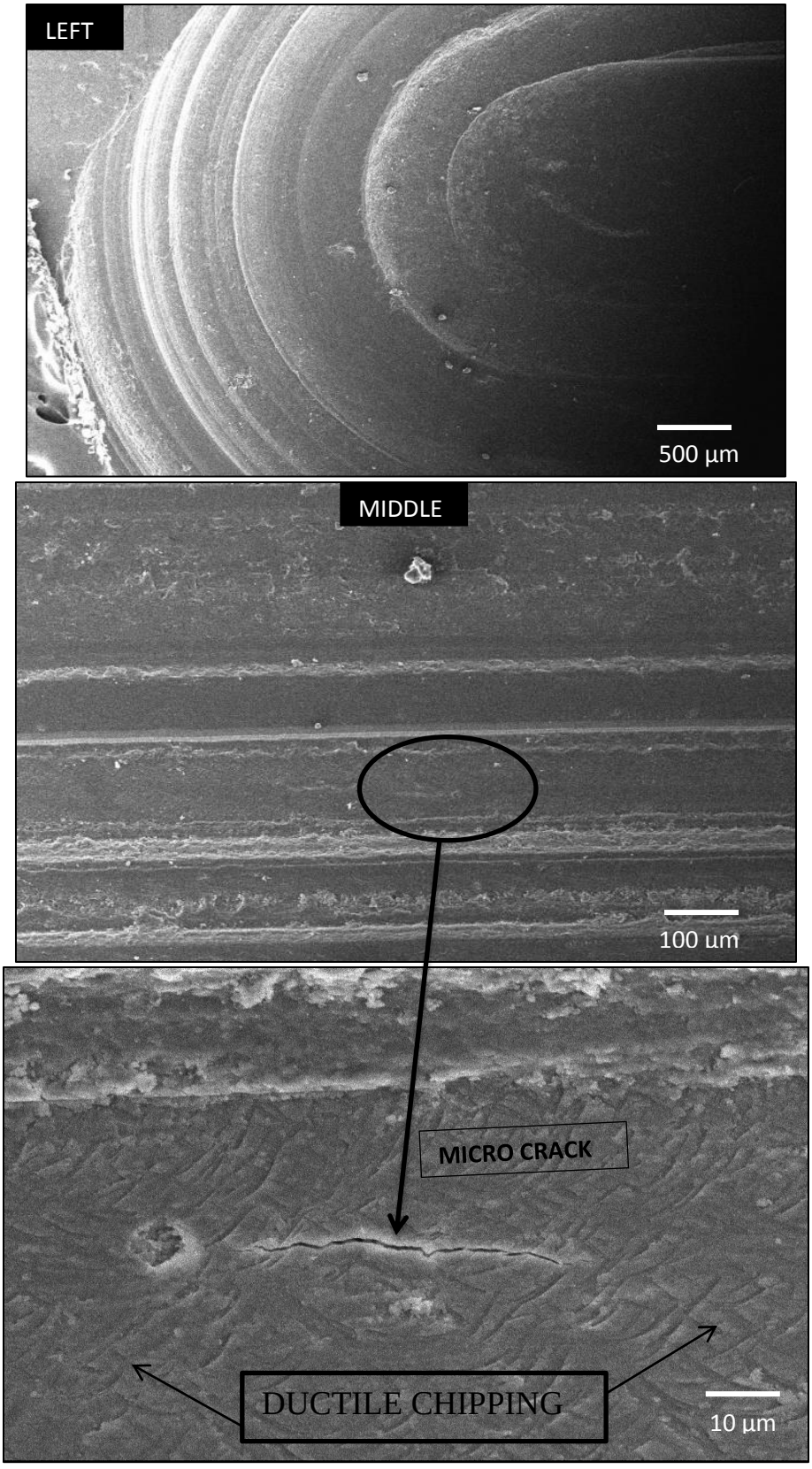

Figure 4.10: Micrographs at spindle speed = 3000 rpm, feed-rate = 2 mm/min and depth of cut = 1 mm

From Figures 4.10 and 4.11, it may be observed that a race-course shaped groove is produced by the grinding; cutting lines made are parallel to each other. In Figure 4.10, in middle, there is a micro crack with all-over abrasive cut marks on the surface surrounding it.

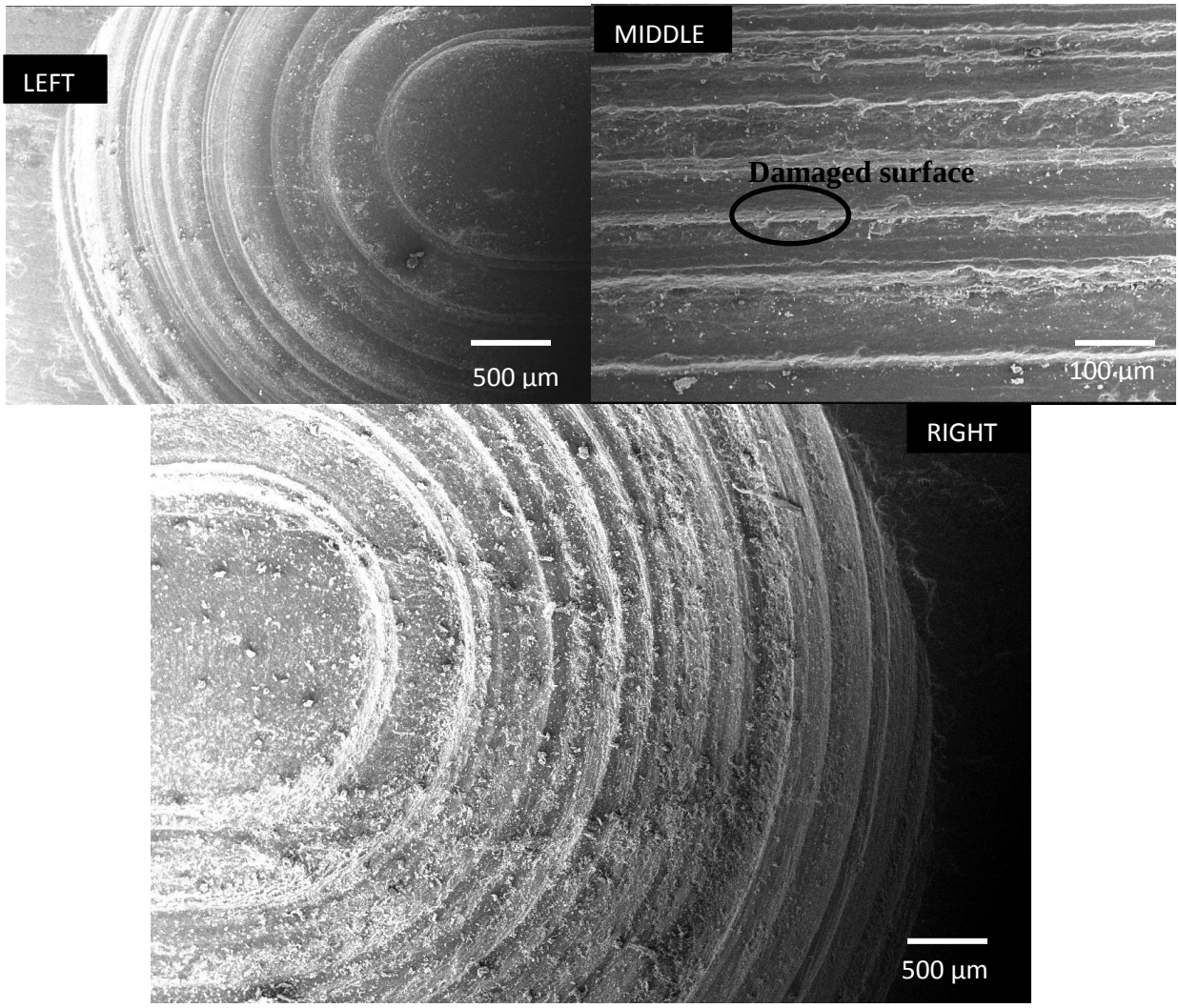

Figure 4.11: Micrographs at spindle speed = 4000 rpm, feed-rate = 1.5 mm/min and depth of cut = 1 mm

It may be observed that in Figure 4.11, extreme left grinded area has smooth surface due to flushing out of the bone debris from grinded area but at the extreme right, when bur leaves surface, the bone debris evacuation, which were at the bur-bone interface, was not done properly leading to poor surface quality.

4.2 Dry (ACRUB + CG)

From DOE in conventional grinding case, although the optimum parameters obtained in first study were A3B1C1 i.e. s= 5000 rpm, f= 1 mm/min and d= 0.5 mm. These parameters are utilized to compare both processes based on thermal temperature, normal force and the surface topography in a single cut because to reduce any effect of bone structural properties when different bone surface is used. No coolant is used.

In this case, first half of length of cut is machined with ACRUB and other half is machined with conventional grinding (CG). The bur is ultrasonically vibrated, which at start moves vertically downward at feed rate 1 mm/min till 0.5 mm depth of cut, then it is made to traverse at same feed rate horizontally up to 5 mm length but in between this length the ultrasonic assistance to bur is switched off. From this point it will cover the remaining distance by conventional grinding of surface. Then it is traversed vertically upwards to reach positive position Z1.

4.2.1 Thermal Analysis

In this case the lowest average temperature (70.54°C) was recorded in area of ACRUB and highest average temperature (74.70°C) in area of conventional grinding. Figure 4.12 illustrates graph of temperature measurement versus frame for this experiment, measured through thermal imager at 8 fps. It may be observed from Figure 4.12 that there are four distinct zones: Zone-1, Zone-2, Zone-3, and Zone-4 i.e. when bur moving vertically downwards, horizontal till the point where ultrasonic vibrations are switched off, then from this point to completion of the length of cut and again moving vertically upwards, respectively. As explained earlier in section 4.1.1, for this experiment, it was decided to consider the minimum value of necrosis, 43°C as shown in Figure 4.12.

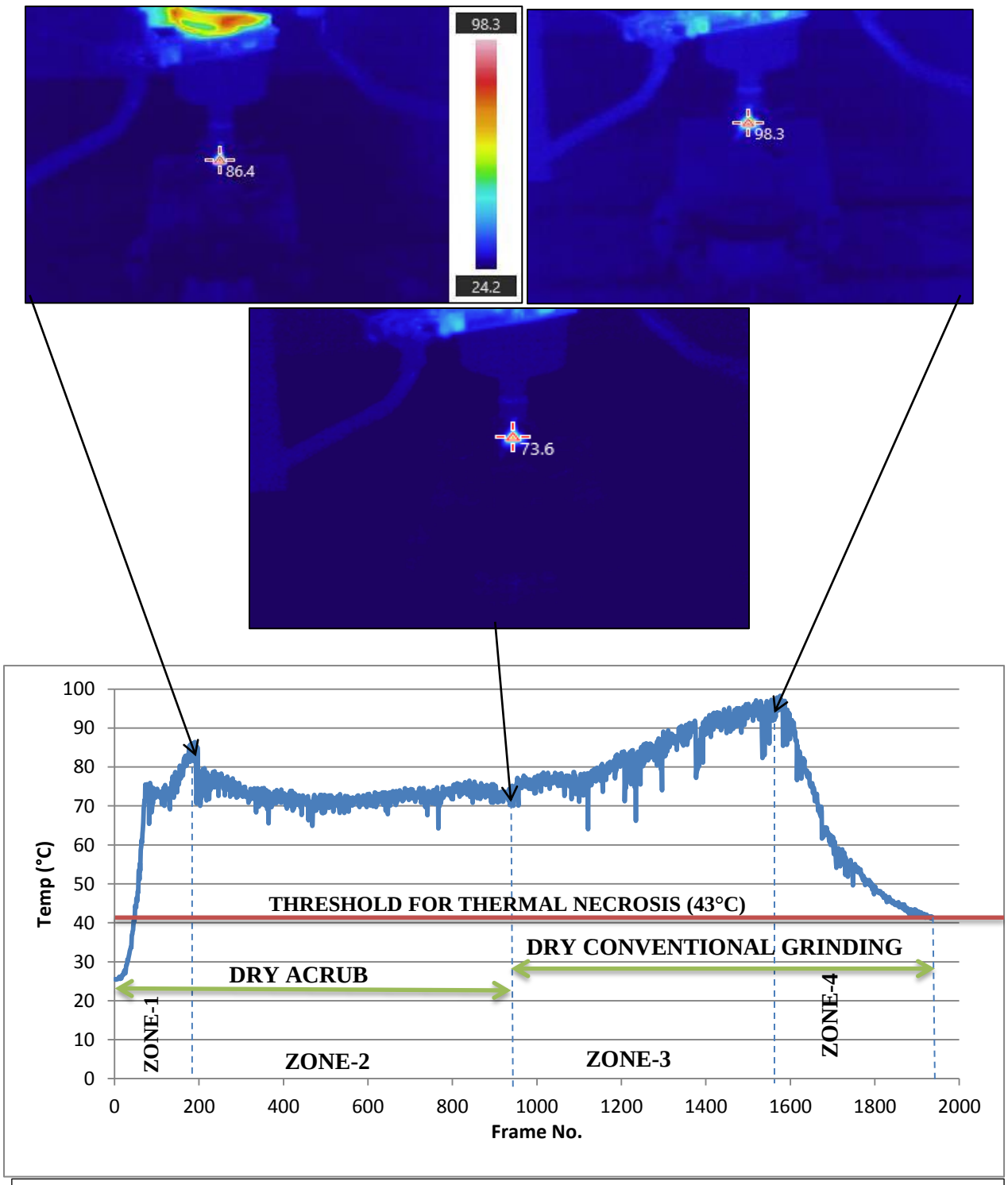

Figure 4.12: Temperature graph for Dry (ACRUB + CG) at s= 5000 rpm, f= 1 mm/min and d= 0.5 mm with thermal images.

In Figure 4.12, at frame no. 1, the ACRUB process starts as this is the point where vibration assisted bur makes contact with the bone. There is rise in temperature till frame no. 190 temperature 86.4°C which is due to bur traversing vertically downwards and there is poor heat loss to surroundings due to very low conductivity of bone, leaving only medium of heat conduction i.e. through bur leading rise to temperature 86.4°C. This temperature is the point where bur has finished 0.5 mm depth of cut. After this point, there is decrease in temperature till frame no. 926 where temperature is 73.6°C, because the bur is now travelling in horizontal direction due to which the area of contact between bur-bone reduces to half of when bur cutting in downward direction resulting in non-contact area open to atmosphere and thus, leading to conduction of heat to air. Then at temperature T_3, there is increase in slope because now the ultrasonic assistance is switched-off, due to which there is rise in temperature till frame no. 1576 where temperature is 98.3°C. Then there is drop in temperature as bur is now traversing vertically upwards, due to which there is no contact between the bur and bone surface and it begins to cool down. The graph covered here is for machining time only.

Above graph states that ACRUB is superior to CG in temperature reduction, although still both violates the threshold of thermal necrosis, because in ACRUB there is very less contact between bur and bone surface as compared to CG due to ultrasonic vibrations. So, lesser the area of contact and contact time lesser will be the frictional force, thus, lower will be the temperature.

4.2.2 Normal Force Analysis

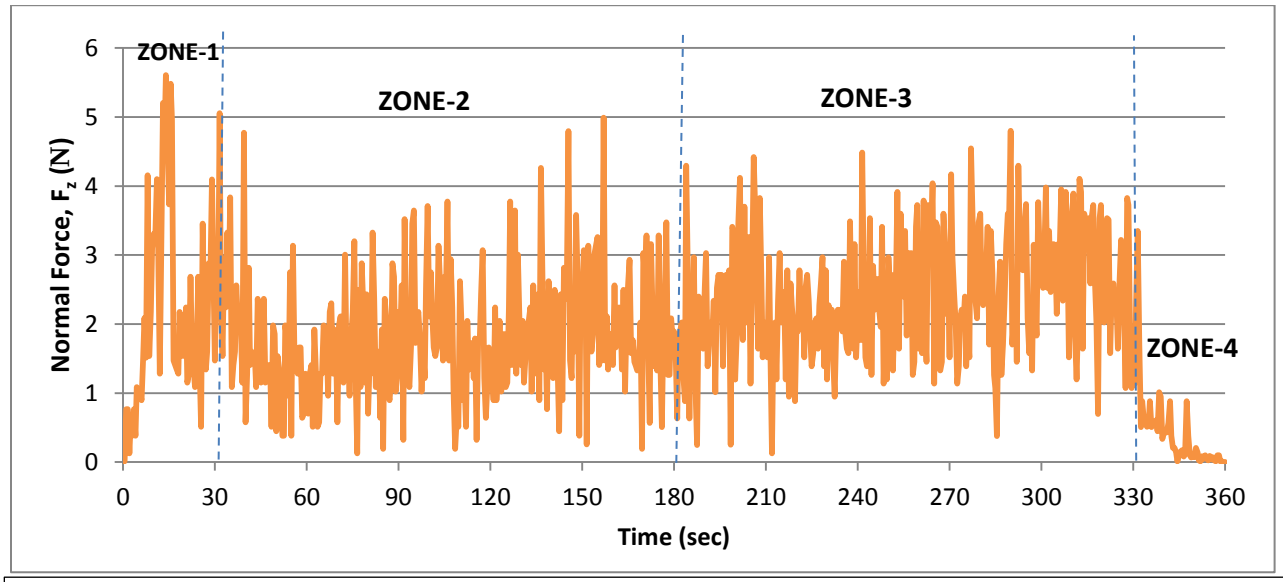

ZONE-1 BUR MOVES VERTICALLY DOWNWARDS ZONE-2 HORIZONTAL MOTION OF BUR WITH ACRUB
ZONE-3 HORIZONTAL MOTION OF BUR WITH CG ZONE-4 VERTICALLY UPWARDS MOTION OF BUR

Figure 4.13: Force versus time graph for Dry (ACRUB+CG) at s= 5000 rpm, f= 1 mm/min and d= 0.5 mm

In this case, it was observed that lowest average normal force was recorded in case of ACRUB (1.88 N) and highest average force CG (2.07 N). Figure 4.13 illustrates graph of normal force measured versus time for this experiment, measured by Dynamometer. It may be observed from Figure 4.13 that when bur starts cutting vertically downwards, the normal force (F_Z) starts increasing and reaches its maximum (5.606 N) at 14^{th} sec, from where it drops down then again moves up till 31.5^{th} sec (5.053 N), where it finishes the 0.5 mm depth of cut, because this is the effect of ultrasonic vibrations on bur which makes the bone debris to escape easily resulting in less exertion of normal force on the bur. Then there is a decrease in average normal force due to movement of bur in horizontal direction till 181.5^{th} sec, where the position of bur is near to length of cut 2.5 mm, because of escaping of bone debris to the free side of the bur. Then there is rise in average normal force due to effect of CG. The force increases till 315.5^{th} sec, then there is small drop in average force till 330.5^{th} sec, where it starts decreasing due to no contact between the bur and bone surface. There is still some force due to presence of bone debris between the bur and grinded surface, as direct contact may not be there, but due to lower rate of increase in gap, thus, bone debris present will have effect on bur.

The graph is evident to the temperature graph in this case that there is direct relationship between force and temperature. This suggests that again ACRUB is better process than CG in terms of both in temperature reduction and in normal force.

4.2.3 SEM Analysis

Figure 4.14 shows the surface topography of both ACRUB and CG. It suggests that dry ACRUB produces good surface finish and dry CG produced poor surface finish.

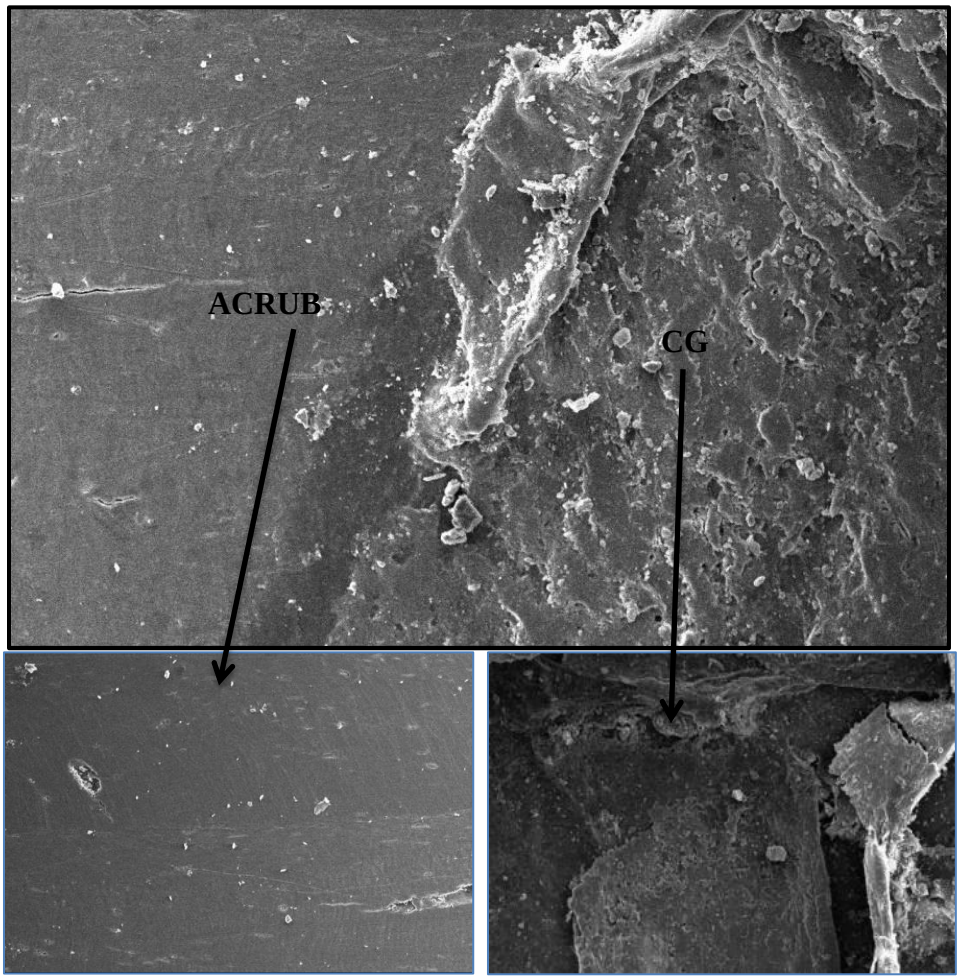

Figure 4.14: Micrographs for dry (ACRUB + CG) at s= 5000 rpm, f= 1 mm/min and d= 0.5 mm

4.3 ACRUB with coolant

Similarly, from section 4.2, in this case also, the experiment will be performed at same parameters i.e. spindle speed, s= 5000 rpm, feed-rate, f= 1 mm/min and d= 0.5 mm used in section 4.2. The diamond bur, 4 mm in diameter, with ultrasonic assisted vibrations first moves vertically downward at 1.5 mm feed rate, then it is made to traverse at same feed rate horizontally up to 5 mm length, and then it is traversed vertically upwards to reach positive position Z1. In this process, the bur-bone interface is continuously fed with water as a coolant to maintain the temperature below the threshold thermal necrosis (43°C) and flush out the bone debris from the grinding area.

4.3.1 Thermal Analysis

Figure 4.15 illustrates graphs of temperature measurement versus frame for this experiment, measured through thermal imager at 8fps. It was found that the average temperature was 25.84013°C and the temperature recorded during whole grinding process was found to be below the threshold line of thermal necrosis set from the literature review i.e. 43°C. It may be observed from Figure 4.13 that the highest temperature observed during the whole process was 31.5°C in frame no. 1106, which is about 27.58% less than the thermal necrosis temperature.

The graph indicates that the ACRUB with coolant is best process for grinding the bone as compared to the first two cases due to its working in very low temperature, free from thermal necrosis.

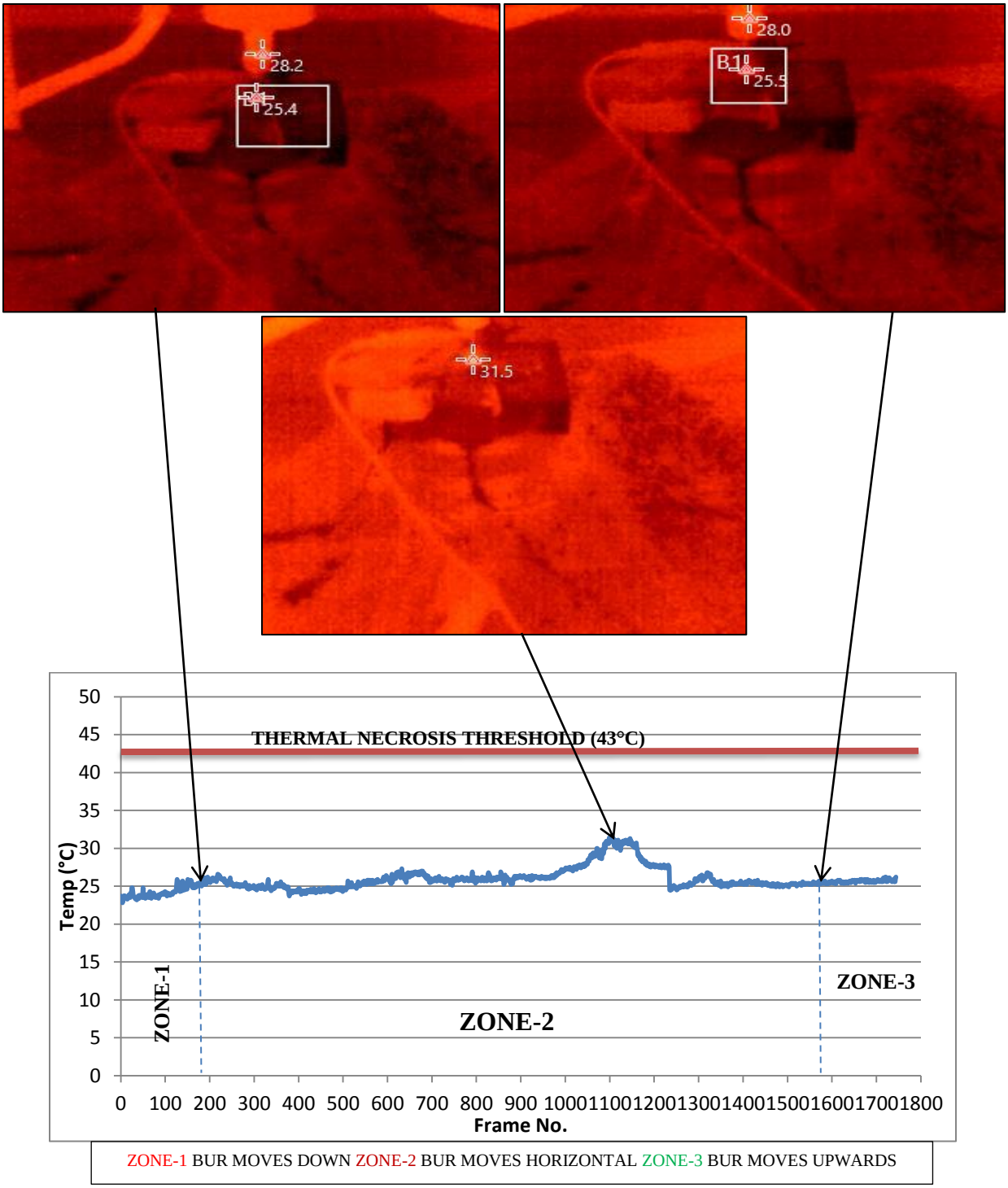

Figure 4.15: Temperature graph in ACRUB with coolant at s= 5000 rpm, f= 1 mm/min and d= 0.5 mm with thermal images.

4.3.2 Normal Force Analysis

The average normal force was calculated from the force readings in this experiment which was found to be 2.465 N. Figure 4.16 shows graphs of force versus time for this experiment, measured by Dynamometer. In Figure 4.16 when vibrations assisted diamond bur starts burring vertically downwards, the normal force (F_Z) starts increasing and reaches 5.94 N at 31.5th sec, where it finishes the 0.5 mm depth of cut. As compared to force graph of section 4.1.2, there is about 23 % reduction in the peak normal force at completion of 0.5 mm depth of cut; this is because the bur is assisted with ultrasonic vibrations of 20,000 Hz due to which the contact is very less with bone surface at an instant as compared to CG, thus lesser will be the force. Now, at this point the bur changes its direction towards horizontal and completes the length of cut at 331.5thsec. It can be observed that the graph has variations in normal force ranging from 0.131–5.67 N, which is not the case in dry ACRUB, also, the average force of dry ACRUB was found to be lesser than ACRUB with support of coolant system; the reason is that the water which is used as a coolant exerts pressure on bur which results in increase of normal forces. It can be seen that there is still some force in zone-3, the reason behind this is the pressure applied by the bone debris and water mixture on bur, even though the bur left the surface but the gap between bur and bone surface is increasing with low rate, thus, strengthening the effect of bone debris-water mixture on bur.

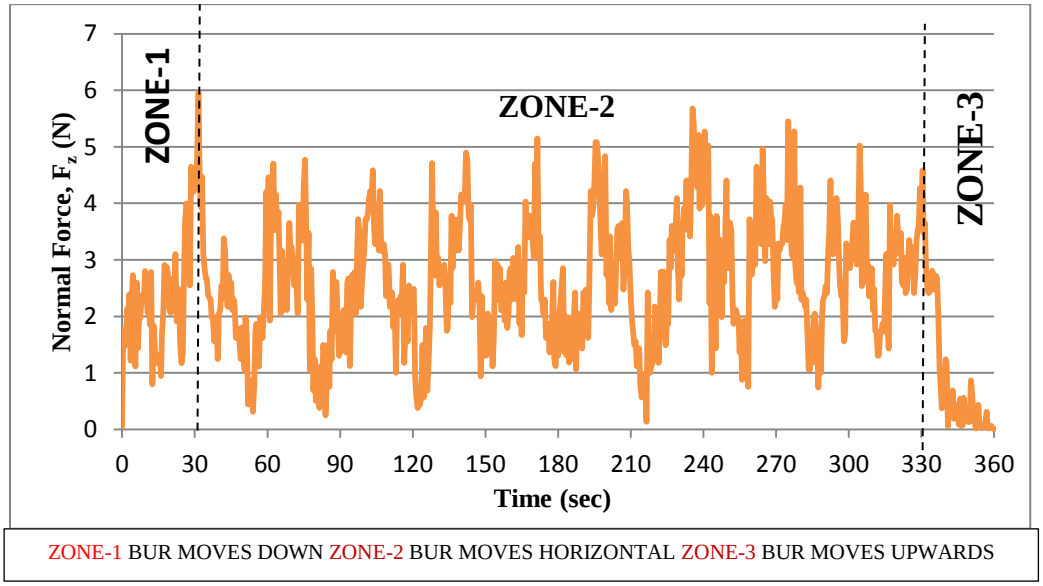

Figure 4.16: Force versus Time graph in ACRUB with coolant at s= 5000 rpm, f= 1 mm/min and d= 0.5 mm

4.3.3 SEM Analysis in ACRUB with coolant

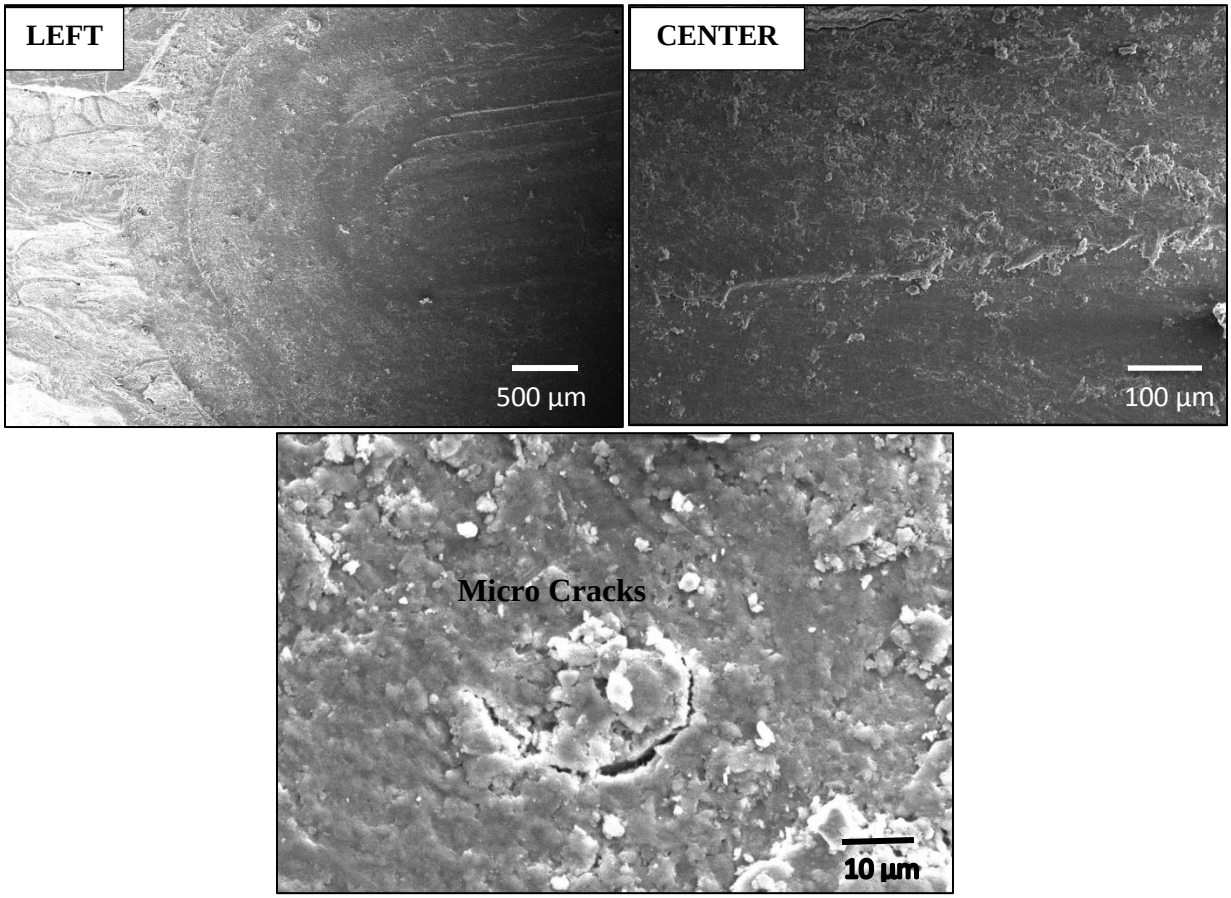

Figure 4.17: Micrographs for ACRUB with coolant at s= 5000 rpm, f= 1 mm/min and d= 0.5 mm

It could be observed from above SEM images that the surface quality was improved. The whiteness on the surface is due to bone swarf getting sticked to the surface on getting wet. There were some micro cracks found on the surface of bone which could be a positively effective in supporting the bone regeneration when a real-life surgery will be performed. It may aid in strength of regenerated bone.

Chapter 5
Conclusion and Future Scopes

5 Conclusion and Future Scopes

5.1 Conclusions

Following conclusions are drawn from the present thesis work:

- An ACRUB setup has been successfully developed to perform surgical operations with precision in control and free from thermal necrosis.
- Temperature and Normal Force has been optimized for input parameters (spindle speed, feed-rate and depth of cut) of dry conventional grinding by using Taguchi L9.
- It was found that depth of cut had major part in increasing the temperature and normal force, after that spindle speed which decreased the temperature and normal forces and then finally, feed-rate which had least contribution in rise of temperature.
- The results obtained from L9 Taguchi experiments, showed that the optimum parameters at smaller the better type for temperature and normal forces were 5000 rpm spindle speed, 1 mm/min feed rate and 0.5 mm depth of cut.
- The temperature graphs of three cases showed that ACRUB with coolant was best with temperatures well below the thermal necrosis threshold i.e. 25.84°C, while other two violated the threshold limit of thermal necrosis.
- The highest temperature observed was 31.5°C in ACRUB with coolant, which was about 27.58% less than the thermal necrosis temperature (43°C).
- The force graphs showed that dry ACRUB (1.88 N) played little better than ACRUB with coolant (2.465 N) in reduction of normal forces as compared to dry conventional grinding.
- The microphotographs obtained from SEM shows that the burred surface produced by conventional grinding was smooth while in ACRUB little rough. And in case of ACRUB with coolant, the surface was with good finish but with white appearance due to adhesion of wet bone swarf to burred surface.

5.2 Future Scopes

- Present study may be helpful for application in dental and neurosurgeries.
- Further research work would be taken out by using materials analogous to bone.
- Further research might be performed by taking other process parameters of ACRUB.
- To conduct ACRUB in orthopedic surgery and neurosurgeries.

References

1. Kondo, S., Okada, Y., Iseki, H., Hori, T., Takakura, K., Kobayashi, A. and Nagata, H., 2000. Thermological study of drilling bone tissue with a high-speed drill. *Neurosurgery*, *46*(5), pp.1162-1168.
2. Sugita, N., Osa, T., Aoki, R. and Mitsuishi, M., 2009. A new cutting method for bone based on its crack propagation characteristics. *CIRP annals*, *58*(1), pp.113-118.
3. Giraud, J.Y., Villemin, S., Darmana, R., Cahuzac, J.P., Autefage, A. and Morucci, J.P., 1991. Bone cutting. *Clinical Physics and Physiological Measurement*, *12*(1), p.1.
4. Abouzgia, M.B. and James, D.F., 1995. Measurements of shaft speed while drilling through bone. *Journal of Oral and Maxillofacial Surgery*, *53*(11), pp.1308-1315.
5. Natali, C., Ingle, P. and Dowell, J., 1996. ORTHOPAEDIC BONE DRILLS–CAN THEY BE IMPROVED?: TEMPERATURE CHANGES NEAR THE DRILLING FACE. *Bone & Joint Journal*, *78*(3), pp.357-362.
6. Bachus, K.N., Rondina, M.T. and Hutchinson, D.T., 2000. The effects of drilling force on cortical temperatures and their duration: an in vitro study. *Medical Engineering and Physics*, *22*(10), pp.685-691.
7. Davidson, S.R. and James, D.F., 2003. Drilling in bone: modeling heat generation and temperature distribution. *Journal of Biomechanical Engineering*, *125*(3), pp.305-314.
8. Matthews, L.S. and Hirsch, C., 1972. Temperatures measured in human cortical bone when drilling. *JBJS*, *54*(2), pp.297-308.
9. Singh, R.P. and Singhal, S., 2016. Rotary ultrasonic machining: a review. *Materials and Manufacturing Processes*, *31*(14), pp.1795-1824.
10. Ngoi, B.K.A. and Sreejith, P.S., 2000. Ductile regime finish machining-a review. *The International Journal of Advanced Manufacturing Technology*, *16*(8), pp.547-550.
11. Chen, J. and De Wolf, I., 2003. Study of damage and stress induced by backgrinding in Si wafers. *Semiconductor science and technology*, *18*(4), p.261.
12. Ethier, C.R. and Simmons, C.A., 2007. *Introductory biomechanics: from cells to organisms*. Cambridge University Press.
13. Wikipedia. Bone. Available at https://en.wikipedia.org/wiki/Bone/ (Accessed on 5th May 2018).

14. Li, X., Zhu, W., Wang, J. and Deng, Y., 2016. Optimization of bone drilling process based on finite element analysis. *Applied Thermal Engineering*, *108*, pp.211-220.
15. Fernandes, M.G., Fonseca, E.M.M., Jorge, R.N., Vaz, M. and Dias, M.I., 2017. Thermal Analysis in Drilling of Ex Vivo Bovine Bones. *Journal of Mechanics in Medicine and Biology*, *17*(05), p.1750082.
16. Shih, A.J., Tai, B.L., Zhang, L., Sullivan, S. and Malkin, S., 2012. Prediction of bone grinding temperature in skull base neurosurgery. *CIRP Annals-Manufacturing Technology*, *61*(1), pp.307-310.
17. KUO, K.L. and TSAO, C.C., 2012. Rotary ultrasonic-assisted milling of brittle materials. *Transactions of Nonferrous Metals Society of China*, *22*, pp.s793-s800.
18. Zhang, L., Tai, B.L., Wang, G., Zhang, K., Sullivan, S. and Shih, A.J., 2013. Thermal model to investigate the temperature in bone grinding for skull base neurosurgery. *Medical Engineering and Physics*, *35*(10), pp.1391-1398.
19. Tai, B.L., Zhang, L., Wang, A., Sullivan, S. and Shih, A.J., 2013. Neurosurgical bone grinding temperature monitoring. *Procedia Cirp*, *5*, pp.226-230.
20. Zhang, L., Tai, B.L., Wang, A.C. and Shih, A.J., 2013. Mist cooling in neurosurgical bone grinding. *CIRP Annals-Manufacturing Technology*, *62*(1), pp.367-370.
21. Enomoto, T., Shigeta, H., Sugihara, T. and Satake, U., 2014. A new surgical grinding wheel for suppressing grinding heat generation in bone resection. *CIRP Annals-Manufacturing Technology*, *63*(1), pp.305-308.
22. Egashira, K., Kumagai, R., Okina, R., Yamaguchi, K. and Ota, M., 2014. Drilling of microholes down to 10 μm in diameter using ultrasonic grinding. *Precision Engineering*, *38*(3), pp.605-610.
23. Jianhua, Z., Yan, Z., Shuo, Z., Fuqiang, T., Lanshen, G. and Ruizhen, D., 2014. Study on effect of ultrasonic vibration on grinding force and surface quality in ultrasonic assisted micro end grinding of silica glass. *Shock and Vibration*, *2014*.
24. Dillon, N.P., Fichera, L., Wellborn, P.S., Labadie, R.F. and Webster, R.J., 2016, October. Making robots mill bone more like human surgeons: Using bone density and anatomic information to mill safely and efficiently. In *Intelligent Robots and Systems (IROS), 2016 IEEE/RSJ International Conference on* (pp. 1837-1843). IEEE.

25. Shen, J.Y., Wang, J.Q., Jiang, B. and Xu, X.P., 2015. Study on wear of diamond wheel in ultrasonic vibration-assisted grinding ceramic. *Wear*, *332*, pp.788-793.
26. Wang, G., Zhang, L., Wang, X. and Tai, B.L., 2016. An inverse method to reconstruct the heat flux produced by bone grinding tools. *International Journal of Thermal Sciences*, *101*, pp.85-92.
27. Liu, W., Deng, Z., Shang, Y. and Wan, L., 2017. Effects of grinding parameters on surface quality in silicon nitride grinding. *Ceramics International*, *43*(1), pp.1571-1577.
28. Yang, M., Li, C., Zhang, Y., Wang, Y., Li, B., Jia, D., Hou, Y. and Li, R., 2017. Research on microscale skull grinding temperature field under different cooling conditions. *Applied Thermal Engineering*, *126*, pp.525-537.
29. Paknejad, M., Abdullah, A. and Azarhoushang, B., 2017. Effects of high power ultrasonic vibration on temperature distribution of workpiece in dry creep feed up grinding. *Ultrasonics sonochemistry*, *39*, pp.392-402.
30. Kusins, J.R., Tutunea-Fatan, O.R. and Ferreira, L.M., 2018. Experimental analysis of the process parameters affecting bone burring operations. *Proceedings of the Institution of Mechanical Engineers, Part H: Journal of Engineering in Medicine*, *232*(1), pp.33-44.
31. Gupta, V. and Pandey, P.M., 2016. An in-vitro study of cutting force and torque during rotary ultrasonic bone drilling. *Proceedings of the Institution of Mechanical Engineers, Part B: Journal of Engineering Manufacture*, p.0954405416673115.

Amanpreet

ORIGINALITY REPORT

11%	3%	9%	4%
SIMILARITY INDEX	INTERNET SOURCES	PUBLICATIONS	STUDENT PAPERS

PRIMARY SOURCES

1	Submitted to Guru Nanak Dev Engineering College Student Paper	3%
2	Singh, Ravi Pratap, and Sandeep Singhal. "Rotary Ultrasonic Machining: A Review", Materials and Manufacturing Processes, 2016. Publication	1%
3	Min Yang, Changhe Li, Yanbin Zhang, Yaogang Wang, Benkai Li, Dongzhou Jia, Yali Hou, Runze Li. "Research on microscale skull grinding temperature field under different cooling conditions", Applied Thermal Engineering, 2017 Publication	1%
4	Wang, Guangjun, Lihui Zhang, Xudong Wang, and Bruce L. Tai. "An inverse method to reconstruct the heat flux produced by bone grinding tools", International Journal of Thermal Sciences, 2016. Publication	<1%